

# Lopingian biotic crisis and global correlation: Evidence from the Abadeh section, central Iran



Dong-xun Yuan <sup>a,b,\*</sup>, Yi-chun Zhang <sup>c</sup>, Mohammad N. Gorgij <sup>d</sup>, Hua Zhang <sup>c</sup>, Lucia Angiolini <sup>e</sup>, Gaia Crippa <sup>e</sup>, Jun Chen <sup>f</sup>, Shu-zhong Shen <sup>b,\*\*</sup>

<sup>a</sup> School of Resources and Geosciences, China University of Mining and Technology, Xuzhou, Jiangsu 221116, China

<sup>b</sup> State Key Laboratory of Critical Earth Material Cycling and Mineral Deposits, School of Earth Sciences and Engineering and Frontiers Science Center for Critical Earth Material Cycling, Nanjing University, Nanjing 210023, China

<sup>c</sup> State Key Laboratory of Palaeobiology and Stratigraphy, Nanjing Institute of Geology and Palaeontology, Chinese Academy of Sciences, Nanjing, Jiangsu 210008, China

<sup>d</sup> Geology Department, Faculty of Sciences, University of Sistan and Baluchestan, Zahedan, Iran

<sup>e</sup> Dipartimento di Scienze della Terra "A. Desio", Via Mangiagalli 34, 20133 Milano, Italy

<sup>f</sup> State Key Laboratory of Deep Earth Processes and Resources, Guangzhou Institute of Geochemistry, Chinese Academy of Sciences, Guangzhou 510640, China

## ARTICLE INFO

Editor: H. Falcon-Lang

**Keywords:**

Lopingian  
Conodonts  
Guadalupian-Lopingian boundary  
Permian-Triassic boundary  
Mass extinction

## ABSTRACT

The Iranian tectonic blocks host well-preserved marine carbonate-dominated Lopingian (Upper Permian) strata, which have been proposed as one of the best international references for the Lopingian in the Tethyan Realm. However, the correlation of the Lopingian between Iran and other regions remains unresolved. The Abadeh section in central Iran is one of the most intensively studied Lopingian sections, yielding abundant conodonts, but with controversial taxonomy. This study presents an updated high-resolution Lopingian conodont succession from the Abadeh section. Fourteen conodont zones have been identified from the middle Abadeh Formation to the basal Elikah Formation, which can be well correlated with conodont successions from South China. Based on the lowest occurrences (LO) of *Clarkina* at the base of Unit 5 at the Abadeh section, the Guadalupian-Lopingian boundary (GLB) is within Unit 4b, much lower than that previously documented. The Wuchiapingian-Changhsingian boundary (WCB) is precisely constrained at 4.9 m below the top of the Hambast Formation. The Permian-Triassic boundary (PTB) is precisely constrained at 0.8 m above the base of the Elikah Formation. In addition, fusuline, ammonoid, and brachiopod biostratigraphy, as well as  $\delta^{13}\text{C}_{\text{carb}}$ ,  $\delta^{18}\text{O}$ , and Sr isotope chemostratigraphy, and magnetostratigraphy of the Abadeh section, are reviewed. As a result, here an integrative multidisciplinary timescale for the Abadeh section has been established. This timescale provides a state-of-the-art temporal framework for both the regional and global correlation of the Lopingian. The integrative fossil ranges at the Abadeh section indicate that the hypothesized end-Guadalupian mass extinction displayed a gradually decline until the middle Wuchiapingian, suggesting a model of protracted ecological turnover rather than a distinct mass extinction event. Whereas, although most of the fossil ranges disappeared before the Changhsingian, the pattern of the end-Permian mass extinction at Abadeh is consistent with all other regions.

## 1. Introduction

The Lopingian Series, the uppermost interval of the Paleozoic Era, is bracketed by two catastrophic biological events: end-Guadalupian mass extinction (EGME, or the pre-Lopingian crisis) (Jin et al., 1994; Stanley and Yang, 1994; Clapham et al., 2009; Chen and Shen, 2019; Rampino and Shen, 2021) and the end-Permian mass extinction (EPME) (Erwin,

1990; Jin et al., 2000; Shen et al., 2011; Fan et al., 2020; Algeo and Shen, 2024). This interval serves as a critical archive for understanding the Paleozoic-Mesozoic transition, including paleoclimate shift (Payne et al., 2010; Jost et al., 2014; Zhang et al., 2018; Chen et al., 2016, 2020; Sun et al., 2024; Viaretti et al., 2025), biodiversity turnover, mass extinction and subsequent restructuring of marine and terrestrial ecosystems (Shen and Shi, 2009; Angiolini et al., 2010; Song et al., 2013;

\* Corresponding author at: School of Resources and Geosciences, China University of Mining and Technology, Xuzhou, Jiangsu 221116, China.

\*\* Corresponding author at: State Key Laboratory of Critical Earth Material Cycling and Mineral Deposits, School of Earth Sciences and Engineering and Frontiers Science Center for Critical Earth Material Cycling, Nanjing University, Nanjing 210023, China.

E-mail addresses: [dxyuan@cumt.edu.cn](mailto:dxyuan@cumt.edu.cn) (D.-x. Yuan), [szshen@nju.edu.cn](mailto:szshen@nju.edu.cn) (S.-z. Shen).

Wang et al., 2014; Stanley, 2016; Chen and Xu, 2019; Shen et al., 2019a, 2020). Establishing a high-resolution global chronostratigraphic framework is therefore pivotal for elucidating the cause-and-effect relationships between environmental perturbations and marine ecosystem collapses during this critical interval.

The Lopingian Series consists of the Wuchiapingian and Changhsingian stages. Three Global Stratotype Sections and Points (GSSPs) for the bases of the Wuchiapingian, Changhsingian and Triassic have been successively defined in South China (Yin et al., 2001; Jin et al., 2006a, 2006b; Shen et al., 2024). The Iranian blocks, on the other hand, situated within the western Paleotethys (or Neotethys referred to Viaretti et al., 2025), also host well-preserved marine Lopingian sequences, which have been the focus of the studies on the Paleozoic-Mesozoic transition (Kozur, 2004, 2005; Shen and Mei, 2010; Arefifard and Payne, 2020; Korn et al., 2021a; Arefifard and Baud, 2022). The Dzhulfian and Dorashamian stages, originally named in Azerbaijan, were proposed as the international standard stages for the Upper Permian (Glenister and Furnish, 1961; Stepanov, 1973; Leven, 1975). Traditionally, the Dzhulfian and Dorashamian stages in Iran have been regarded as equivalent to the Wuchiapingian and the Changhsingian

stages in South China, respectively. However, discrepancies in biostratigraphy and regional correlations have long been a topic of debate (Zhao et al., 1981; Kozur, 2004, 2005; Shen and Mei, 2010).

A series of sections at Abadeh in central Iran have been studied by different research groups, and abundant data were presented, including multiple fossils (Bando, 1979; Iranian-Japanese Research Group (IJRG), 1981; Baghbani, 1993; Kozur, 2004, 2005; Shen and Mei, 2010; Shahinfar et al., 2020; Viaretti et al., 2021; Arefifard and Baud, 2022), magnetostratigraphy (Gallet et al., 2000), and multiple isotopic chronostratigraphy (Korte et al., 2003, 2004; Richoz et al., 2010; Liu et al., 2013; Shen et al., 2013; Dudás et al., 2017; Chen et al., 2020; Viaretti et al., 2025). Among these, conodonts are the most abundant fossils at the Abadeh section and provide the primary basis for the global correlation of the Lopingian. Nevertheless, high-resolution samples through the entire Lopingian in central Iran is lacking prior to our study and a part of the conodont taxonomic identifications remain controversial (Kozur, 2004, 2005; Shen and Mei, 2010).

To address these issues, we herein present a comprehensive Lopingian conodont biostratigraphical framework for the Abadeh section based on high-resolution conodont samples collected during three field

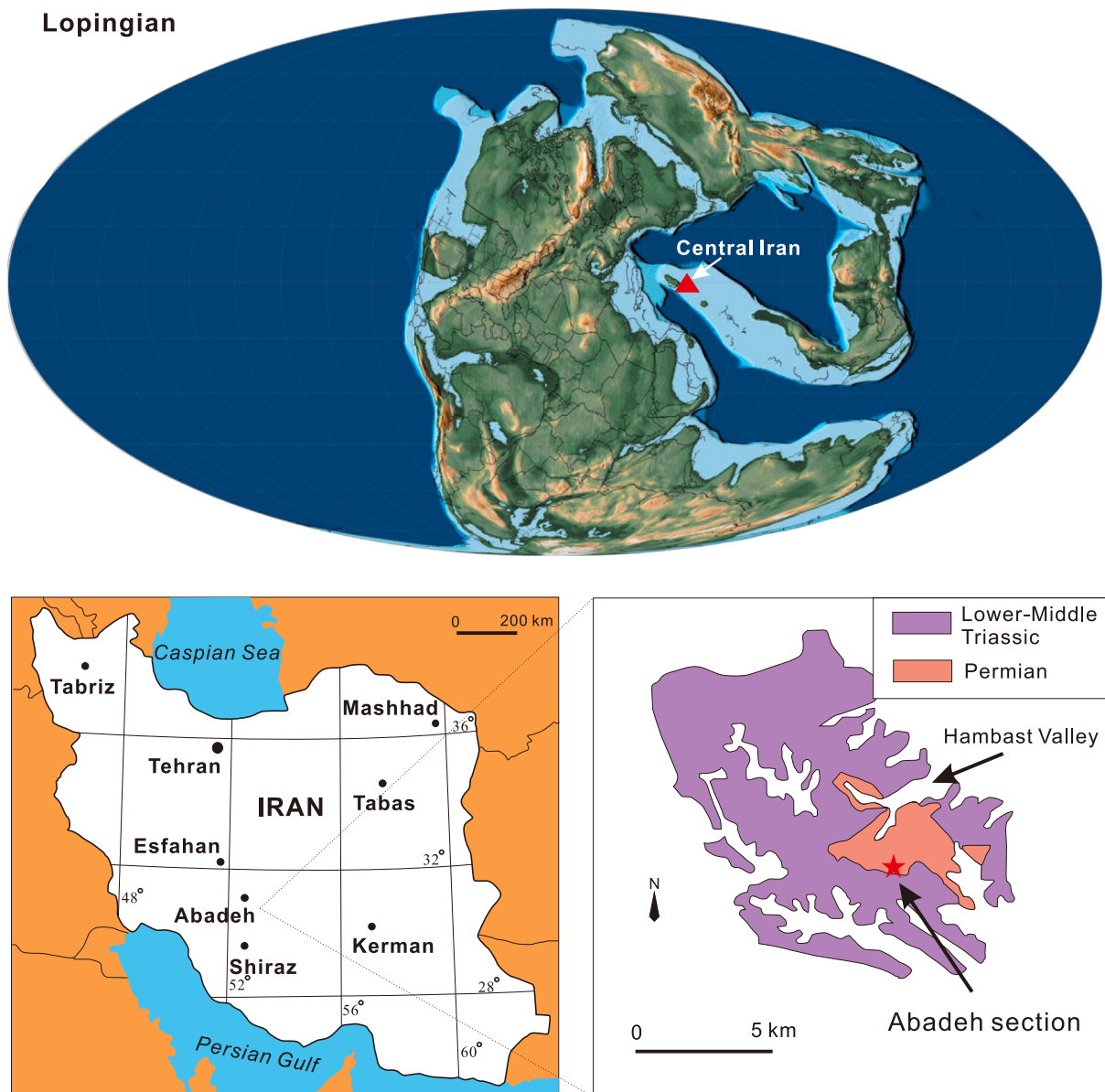
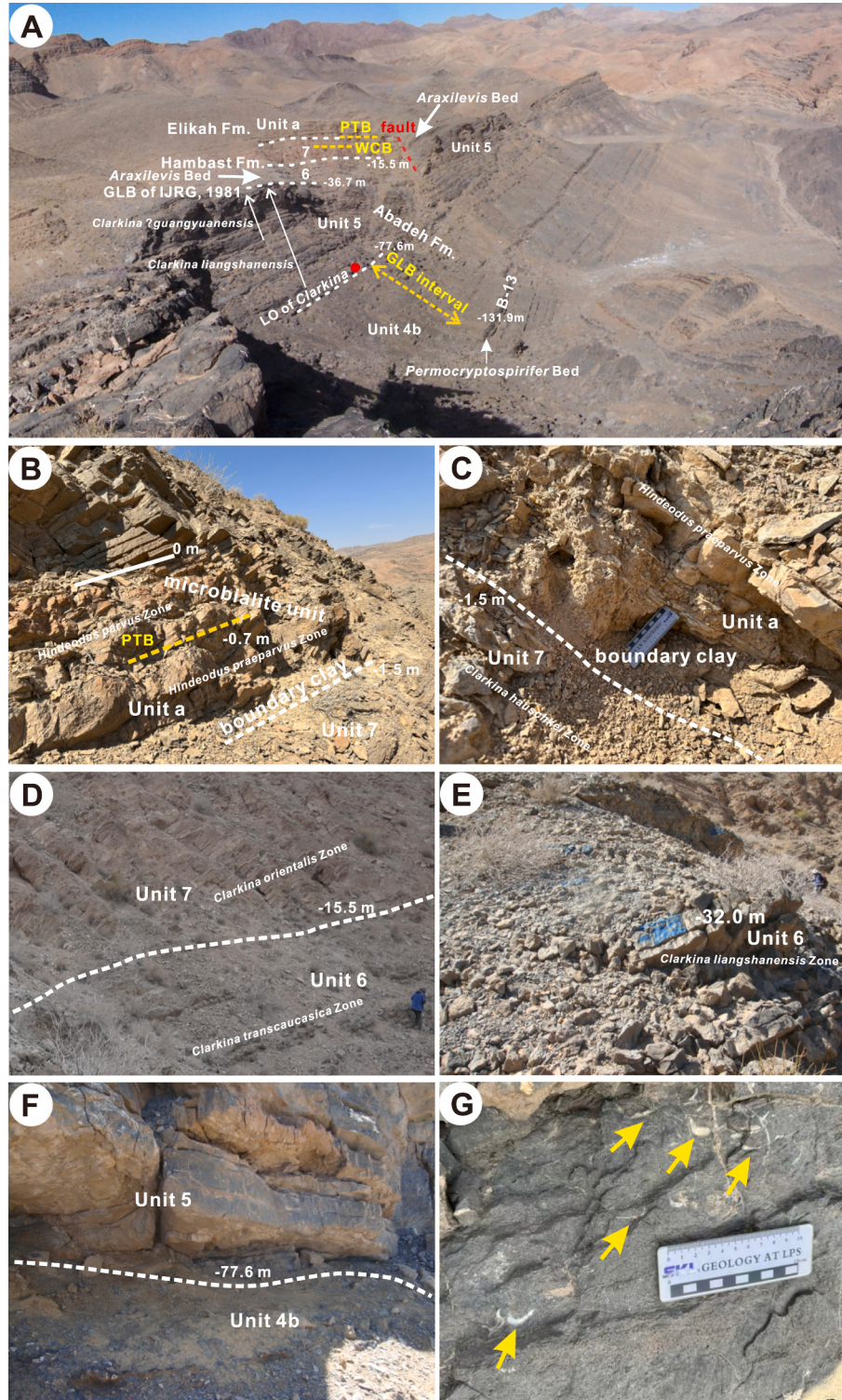


Fig. 1. Locality and reconstruction maps showing the position of the Abadeh section (IJRG, 1981; Scotese, 2014).

excursions between 2009 and 2023, and integrate a high-resolution Lopingian timescale for Abadeh to facilitate correlation with the Lopingian in South China and other regions. Furthermore, based on all the fossil records constrained by our new timescale, the process and potential relationship of the two Lopingian biotic crises have been proposed at Abadeh.

## 2. Geological setting and stratigraphy

The Central Iran Block represents an important part of the western Cimmerian blocks and drifted away from the Gondwana margin during the middle-late Cisuralian (Early Permian) (Şengör, 1979). It is particularly notable for its continuous marine carbonate-dominated sequences spanning the Cisuralian to Middle Triassic, offering ideal multiple



**Fig. 2.** Outcrops of the Abadeh section. (A) exposure between the upper Abadeh and the basal Elikah formations at Abadeh, (B) the boundary between Units 7 and a, and Microbialite Bed, (C) Boundary Clay, (D) Unit 7 and boundary between Units 6 and 7, (E) the lower part of Unit 6, (F) the boundary between Units 4b and 5, (G) bed with the Guadalupian brachiopod *Permocryptospirifer* at 54.3 m below the top Unit 4b in the upper Abadeh Formation.

sections (e.g., Abadeh, Shahreza and Baghuk Mountain sections) for correlation with the Lopingian of South China and other regions (IJRG, 1981; Zhao et al., 1981; Shen and Mei, 2010; Korn et al., 2021a, 2021b). The Abadeh section of this study is located in the Hambast Valley, near the border between Yazd and Fars provinces, approximately 60 km southeast of Abadeh, Fars Province. Paleogeographically, this section was situated in the Central Iran Block within the tropical western Paleotethys-Neotethys during the Lopingian (Fig. 1).

Taraz (1969, 1971, 1974) initially documented the Abadeh section, subdividing its Permian and Triassic sequences into 12 lithologic units. Subsequently, the Iranian-Japanese Research Group reclassified these sequences into four distinct formations, the Surmaq (Units 1 to 3), Abadeh (Units 4a, 4b, 5), Hambast (Units 6, 7) and Elikah (Units a-e) formations in ascending order (Fig. 2; IJRG, 1981). The Surmaq Formation exceeds 450 m in thickness, consisting primarily of grey limestones interbedded with shales and chert bands or nodules. The Abadeh Formation, approximately 458 m thick, is characterized by the presence of thick, black, flaggy shales, with more limestones in its upper part. The overlying Hambast Formation, about 35 m thick, is mostly composed of variegated rocks, including grey-reddish limestones and greenish-reddish shales (Fig. 2A). The basal Elikah Formation (Unit a) is marked by a boundary clay (Fig. 2C) and a microbialite unit (Fig. 2B) at the base. It is about 90 m thick and consists of yellow to grey thin-

bedded vermicular limestones interbedded with shales (IJRG, 1981).

We successively investigated the Abadeh section in the Hambast Valley during the field trips in 2009, 2017, and 2023, and measured the section from the base of the Abadeh Formation to the lowest part of the Elikah Formation (Fig. 2A; Shen et al., 2009; Angiolini et al., 2017). We started the measurement of the section from the top of the microbialite unit of the Elikah Formation (0 m), consistent with that of Dudás et al. (2017) and Chen et al. (2020). The base of Unit a (the basal part of the Elikah Formation) is at  $-1.5$  m; Unit 7 ranges from  $-15.5$  m to  $-1.5$  m; Unit 6 is between  $-36.7$  m and  $-15.5$  m; and the boundary between Unit 5 and Unit 4b is at  $-77.6$  m (Fig. 2).

### 3. Conodont succession

A total of 200 conodont samples were collected from an interval of approximately 83 m thickness from the base of Unit 5 of the Abadeh Formation to Unit 6 of the Elikah Formation at the Abadeh section. Of these, 161 samples are productive (Fig. 3). Abundant conodonts were yielded, particularly from the upper part of Unit 5 and the Hambast Formation, and most of them are P<sub>1</sub> elements. Twenty-five species of five genera were identified (Figs. 4–10). Based on these materials, fourteen conodont interval zones, defined by the lowest occurrences (LOs) of the index species and ended by the next index species, have been

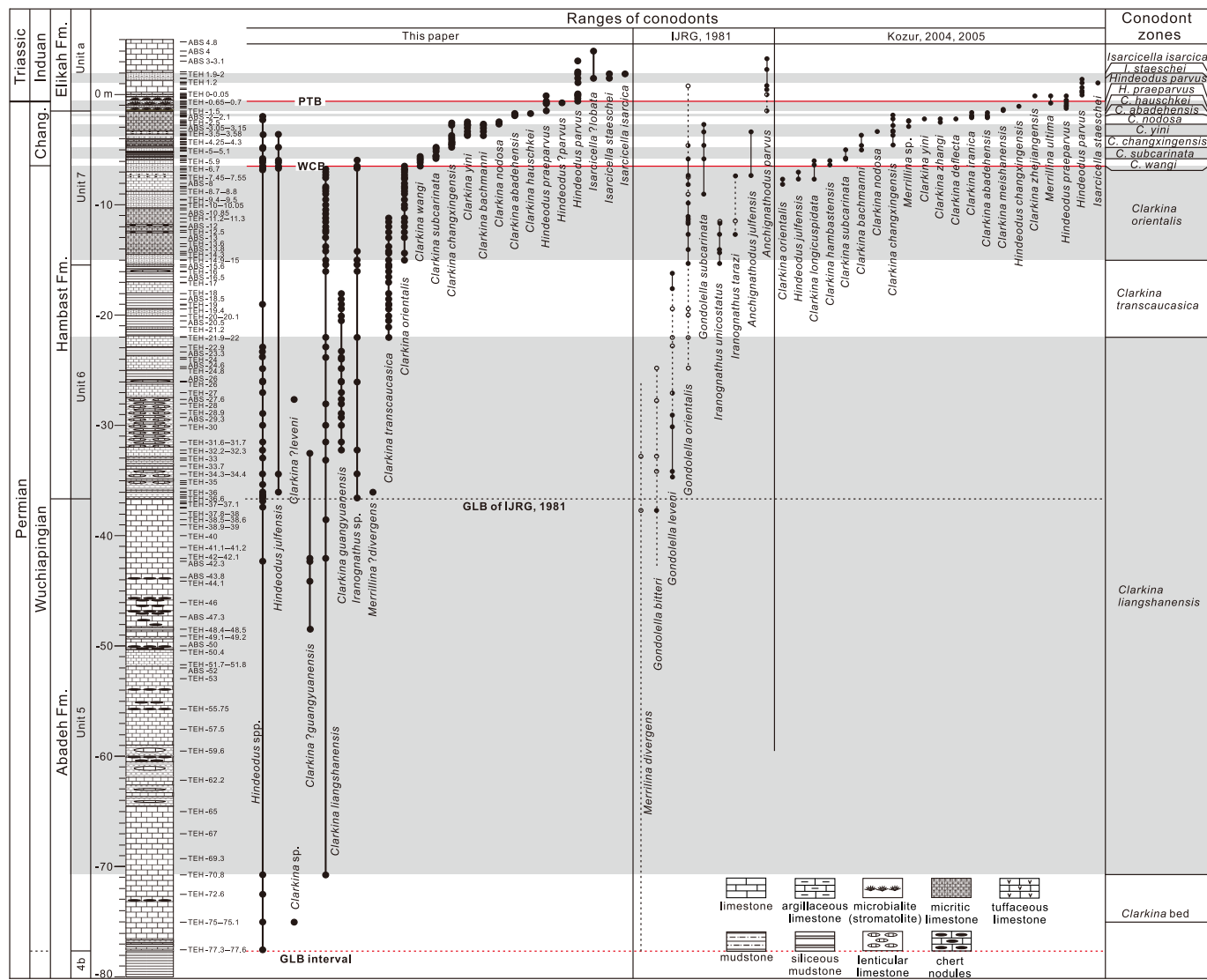


**Fig. 3.** Ranges of conodont species and zones for the Lopingian at the Abadeh section.

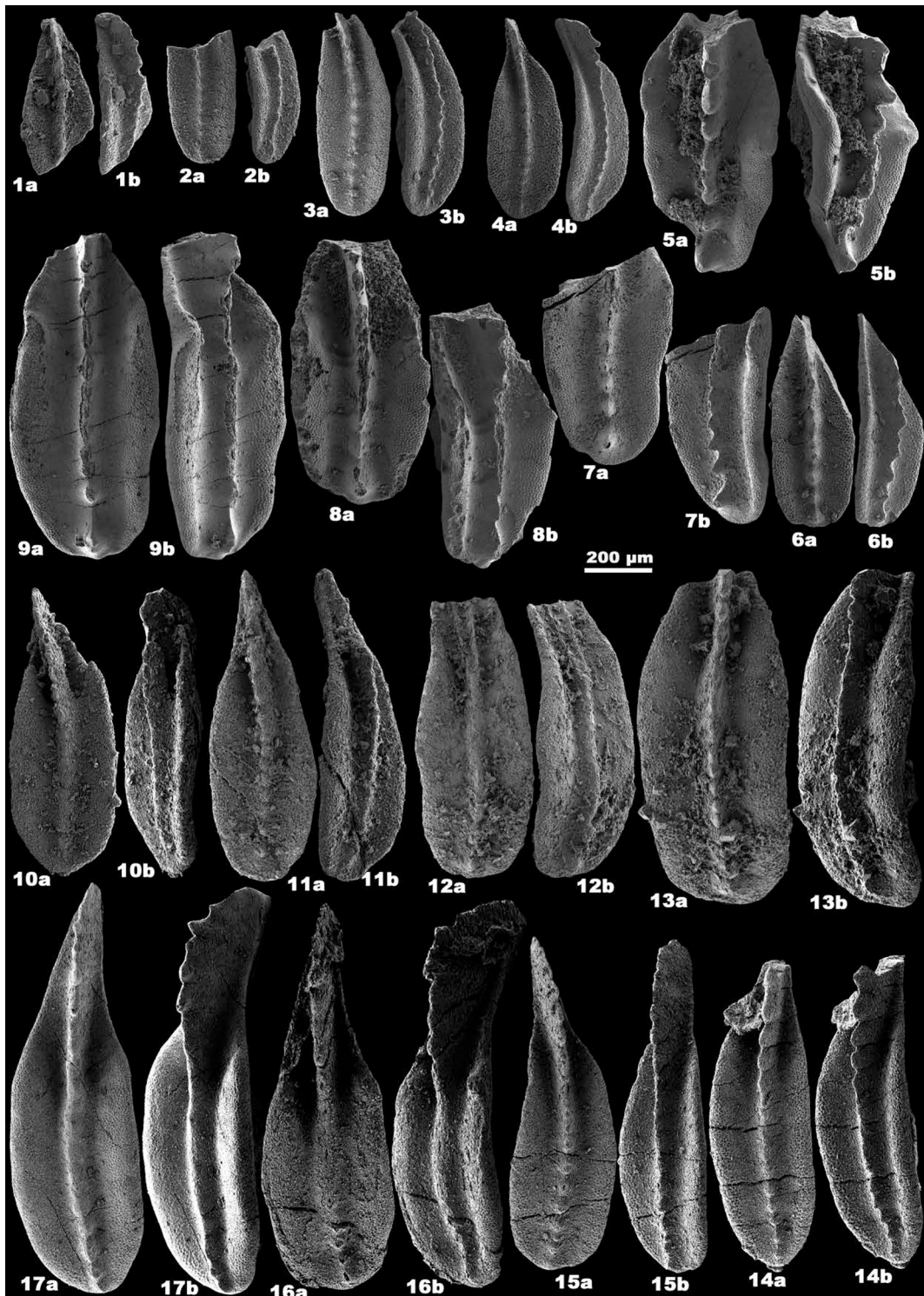


**Fig. 4.** 1. *Clarkina* sp., from sample TEH -75~75.1 m. 2–4. *Clarkina* ?*liangshanensis*, from sample TEH -70.8 m. 5–9. *Clarkina* ?*guangyuanensis*, 5 from sample TEH -48.4~48.5 m; 6, 7 from sample TEH -42~42.1 m; 8, 9 from sample ABS -42.3 m. 10–17. *Clarkina liangshanensis*, 10, 11 from sample TEH -38.5~38.6 m; 12, 13 from sample TEH -31.6~31.7 m; 14–17 from sample ABS -13 m.

recognized. They are the *Clarkina liangshanensis*, *C. transcaucasica*, *C. orientalis*, *C. wangi*, *C. subcarinata*, *C. changxingensis*, *C. yini*, *C. nodosa*, *C. abadehensis*, *C. hauschkei*, *Hindeodus praeparvus*, *H. parvus*, *Isarcicella staeschei* and *I. isarcica* zones in ascending order, as described in details below and illustrated in Fig. 3.

### 3.1. *Clarkina liangshanensis* Zone (base uncertain to Sample TEH -21.9 ~-22 m)

This zone extends from the basal part of Unit 5 to the middle part of Unit 6. The lower and middle parts of Unit 5 yielded rare conodonts, resulting in some species-level identification uncertainty, and some broken primitive *Clarkina* ?*liangshanensis* (Figs. 4.2–4.4) and *C. ?*

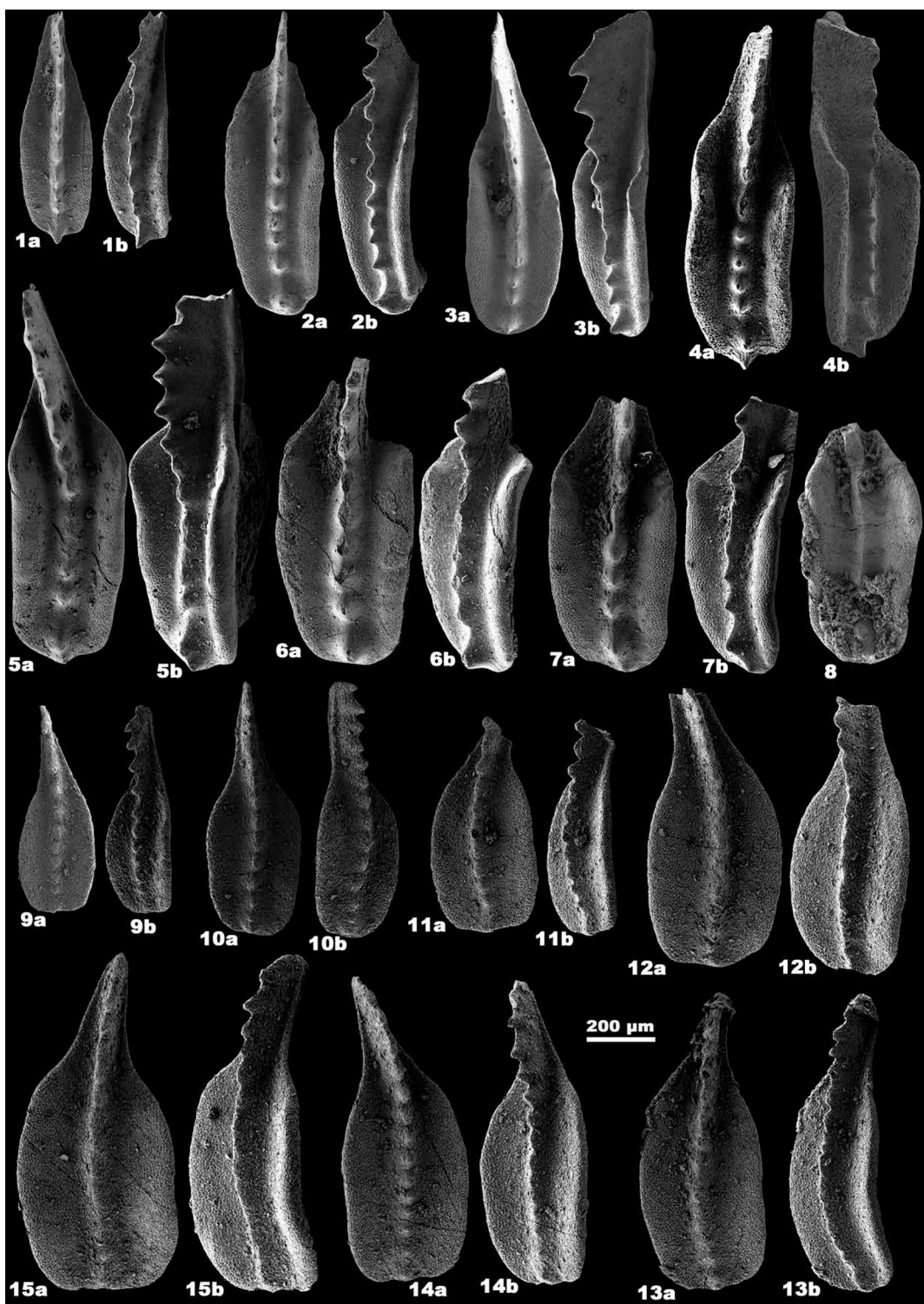


**Fig. 5.** 1–8. *Clarkina guangyuanensis*, 1–7 from sample TEH -27 m; 8 from sample ABS -27.6 m. 9–15. *Clarkina transcaucasica*, from sample TEH -21.9–22 m.

*guangyuanensis* (Figs. 4.5–4.9) were found. Unit 6 yielded abundant conodonts which provide reliable species identification and recognition of the zone. In addition to *C. liangshanensis*, some *Hindeodus julfensis*, *Iranognathus* sp. and abundant *Clarkina guangyuanensis* were also present in the zone.

The LO of *Clarkina liangshanensis* generally coincides with the LO of *C. guangyuanensis* at many sections in South China, making the *C. liangshanensis* Zone is roughly equivalent to the *C. guangyuanensis* Zone at these sections (Shen et al., 2010; Yuan et al., 2017, 2019). Shen

and Mei (2010) recognized the *C. guangyuanensis* Zone at the Abadeh section based on the specimens reported by IJRG (1981).

IJRG (1981) established the *Merrillina divergens* Zone in the lower part of this interval. However, all their samples yielding *M. divergens* are near the boundary between Units 5 and 6, and no *M. divergens* specimens were found within their *M. divergens* Zone (Figs. 3, 11). This study also found a *M. ?divergens* specimen at the base of Unit 6 (Fig. 10.29), confirming its presence as reported by IJRG (1981).

IJRG (1981) also established the *Gondolella* (=*Clarkina* in this study)

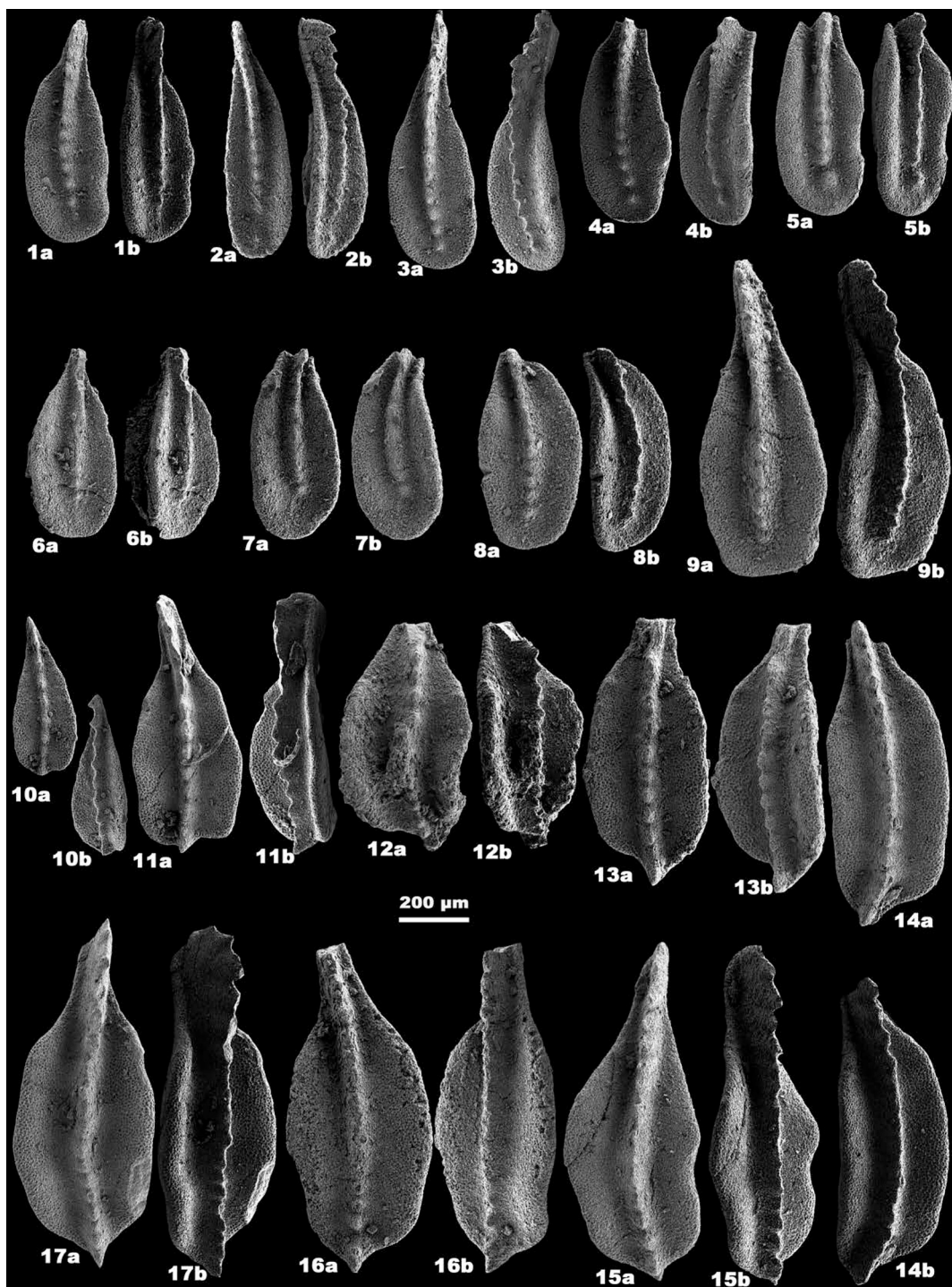


**Fig. 6.** 1–9. *Clarkina orientalis*, 1–5 from sample ABS -8.5 m; 6–9 from sample ABS -8.0 m. 10–17. *Clarkina wangi*, from sample ABS -6.4 m.

*bitteri* and *G. leveni* zones from the uppermost Unit 5 to the top of Unit 6. The *G. bitteri* Zone of IJRG (1981) is roughly equivalent to the middle part of the *Clarkina liangshanensis* Zone in this study (Fig. 11). *Gondolella bitteri* was first described in Nevada, USA by Kozur (1975), and Wang and Wang (1981) established *Neogondolella* (=*Clarkina* in this study) *liangshanensis-N. bitteri* Assemblage Zone in China, which was considered to represent the lower Wuchiapingian Stage. However, Mei and Wardlaw (1996) argued that *N. bitteri* is a cool water species of late Wordian age, advocating for the abandonment of the assemblage zone. The LO of *Clarkina leveni* in IJRG (1981) is higher than the LO of *C. liangshanensis* in our study, and some questionable *C. orientalis* were

reported in their *C. leveni* Zone by IJRG (1981). Shen and Mei (2010) also recognized the *C. leveni* Zone at this section (Fig. 11). The *C. leveni* Zone is generally regarded as a zone below the *C. liangshanensis* Zone or the *C. guangyuanensis* Zone in South China (Mei et al., 1994a, 1994b, 1998; Shen et al., 2010; Yuan et al., 2017, 2019). The reported range of *C. leveni* in both IJRG (1981) and Shen and Mei (2010) overlaps within the *C. liangshanensis* Zone in this study (Fig. 3). In addition, a few *C. ? leveni* were found in one sample within the *C. liangshanensis* Zone, and we here assign the horizon containing these *C. leveni* specimens to the *C. liangshanensis* Zone.

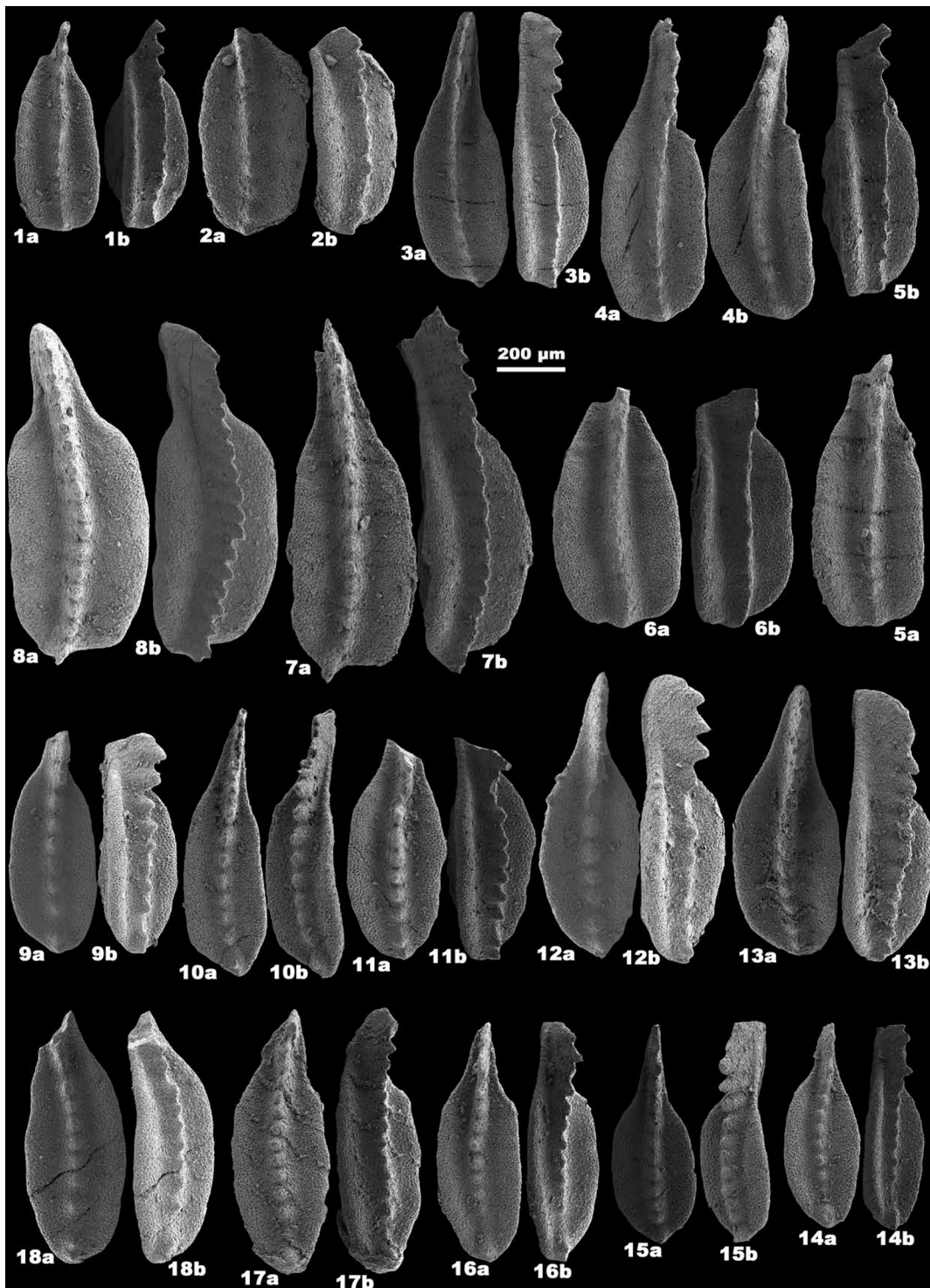


**Fig. 7.** 1–8. *Clarkina subcarinata*, from sample ABS -5.5 m. 9–18. *Clarkina changxingensis*, 9–13 from sample TEH -4.5~--4.55 m; 14–18 from sample TEH -4.25~--4.3 m.

### 3.2. *Clarkina transcaucasica* Zone (Sample TEH -21.9~--22 m to TEH -15 m)

This zone ranges from the upper part of Unit 6 to the basal Unit 7. *Clarkina liangshanensis*, *Hindeodus* sp. and *Iranognathus* sp. coexist with *Clarkina transcaucasica*, and some *C. guangyuanensis* can still be found in the lower part of this zone. Some *Clarkina* specimens in this zone exhibit a relatively wide posterior brim, but the characters of their denticles in the middle and posterior part and posterior end of the platform are

consistent with those of *C. transcaucasica*.

IJRG (1981) also found a few *Clarkina orientalis* in this interval, marked with hollow circles in their Fig. 8 (see Fig. 3 in this study). However, they did not designate this interval as the *C. orientalis* Zone, probably because these specimens were not considered as typical *C. orientalis*. Gullo and Kozur (1992) split *C. orientalis transcaucasica* from *C. orientalis*, and these atypical *C. orientalis* in this interval at the Abadeh section were referred to *C. transcaucasica* (Mei et al., 1994a; Shen and Mei, 2010; Yuan et al., 2017), which corresponds to the

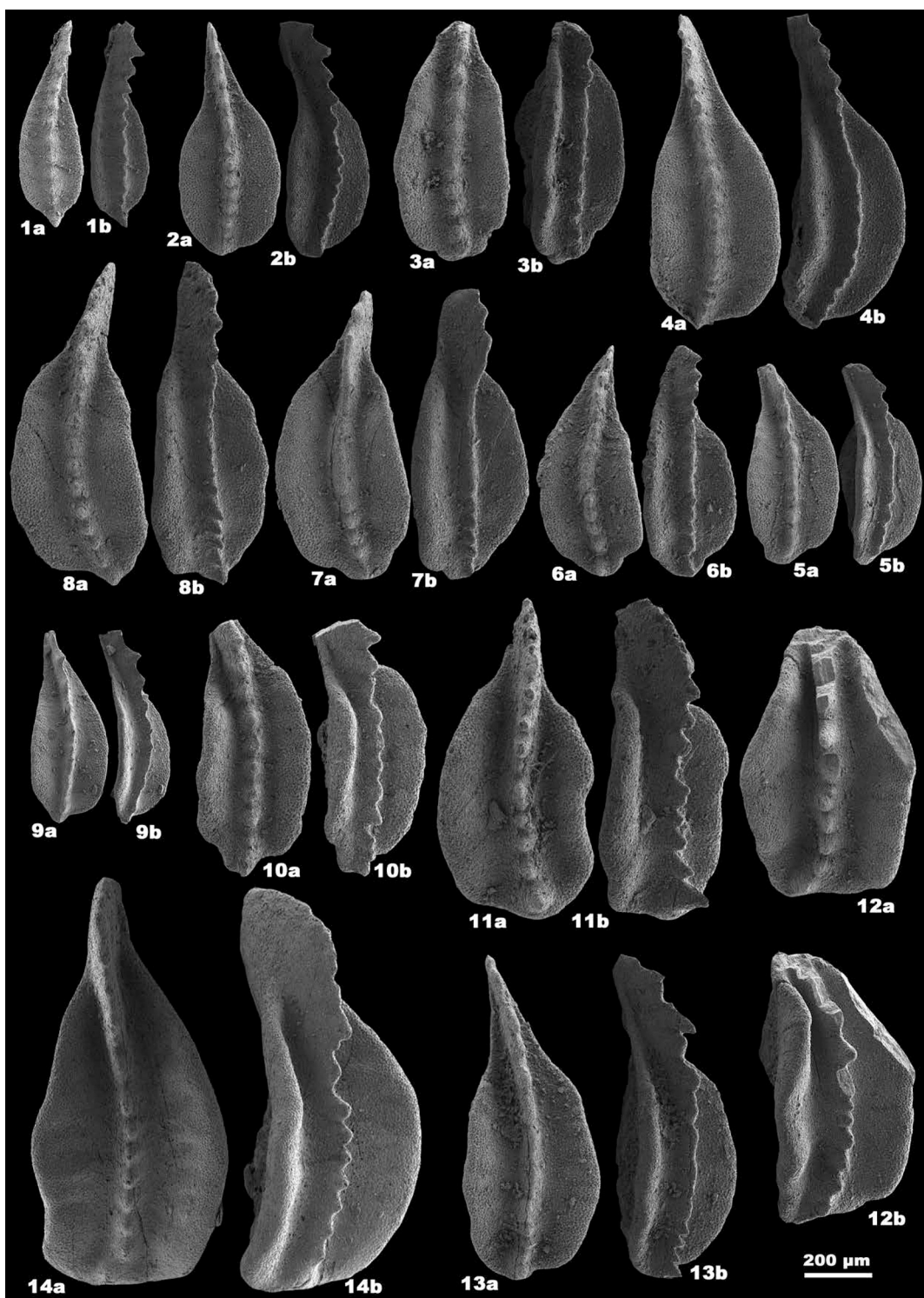


**Fig. 8.** 1–8. *Clarkina yini*, 1, 2, 4 from sample TEH -3.7 m; 3 from sample ABS -3.35 m; 5–8 from sample TEH -2.8 m. 9–15. *Clarkina bachmanni*, 9–12 from sample ABS -2.8 m; 13 from sample TEH -2.8 m; 14 from sample ABS -2.7 m.

*C. transcaucasica* Zone in this study. Shen and Mei (2010) also recognized this zone above the *C. guangyuensis* Zone at the section, but their boundary between the two zones was uncertain due to rare samples.

### 3.3. *Clarkina orientalis* Zone (Sample TEH -15 m to ABS -6.4 m)

This zone roughly corresponds to the lower part of Unit 7, which yielded abundant *Clarkina* elements, including *C. liangshanensis* existing

in the entire zone and *C. transcaucasica* in its lower part. *Hindeodus julfensis* and *Iranognathus* sp. also coexist with *Clarkina orientalis*.

The base *Clarkina orientalis* Zone of IJRG (1981) is nearly same as this study (Figs. 3, 11). However, the top of this zone of IJRG (1981) was defined by the LO of *Hindeodus julfensis*, which is around the base of Unit 6 in this study, significantly lower than that in IJRG (1981). Therefore, it is inappropriate to use the LO of *H. julfensis* to define the top of the *Clarkina orientalis* Zone. In addition, IJRG (1981) also found some

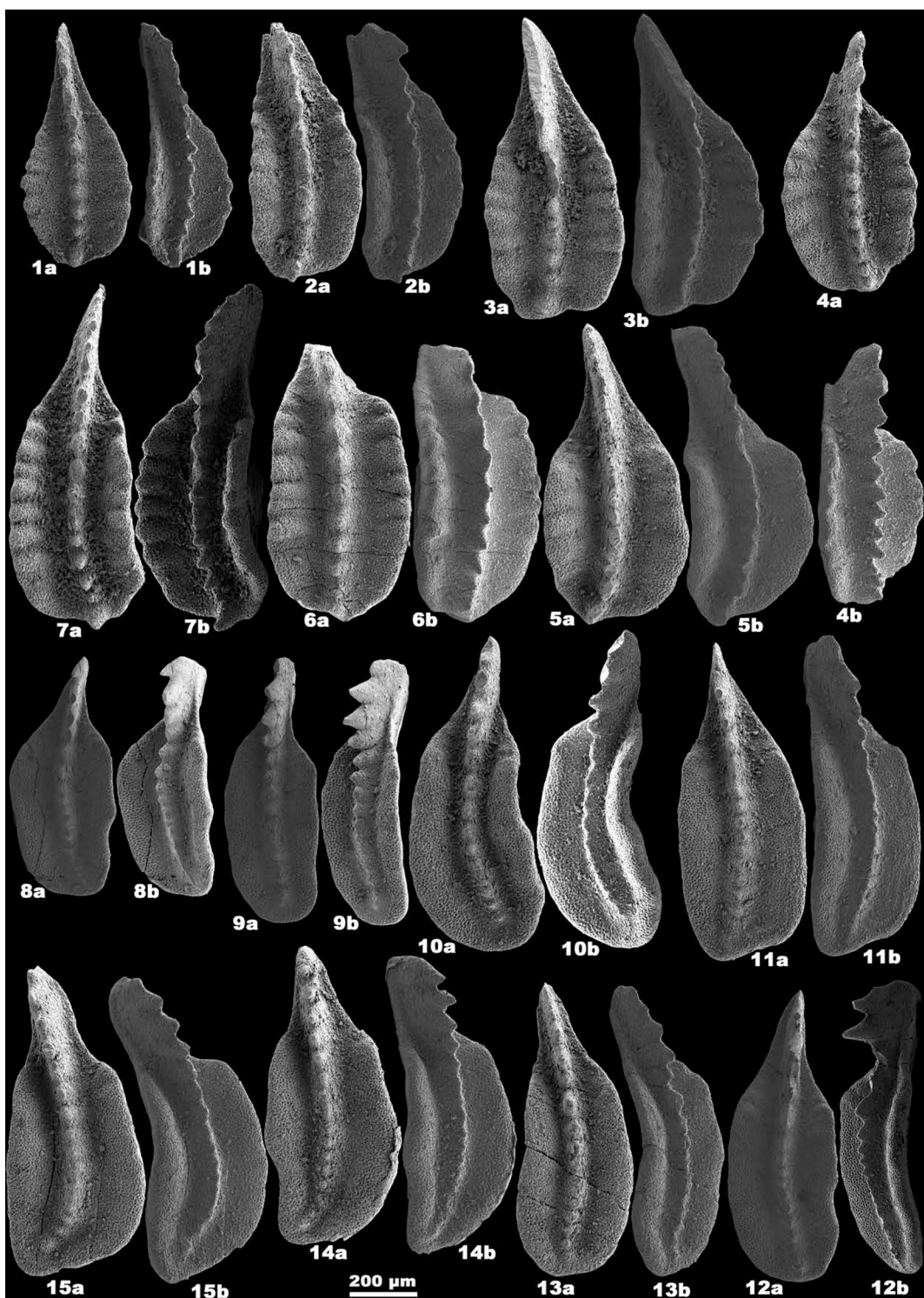


**Fig. 9.** 1–7. *Clarkina nodosa*, from sample TEH -2.5 m. 8–15. *Clarkina abadehensis*, from sample ABS -1.85~--1.9 m.

*Iranognathus unicostatus* and *I. tarazi* in this zone. The top of the *Clarkina orientalis* Zone in Kozur (2005) is consistent with this study. Kozur (2004, 2005) reported a few *Hindeodus julfensis* and *Clarkina longicuspisata*, and established the *C. longicuspisata* Zone above the *C. orientalis* Zone at the section, but no specimens were illustrated. We consider the *C. longicuspisata* Zone of Kozur (2005) to correspond to the topmost part of the *C. orientalis* Zone in this study.

#### 3.4. *Clarkina wangi* Zone (Sample ABS -6.4 m to TEH -5.75 m)

This zone is in the upper part of Unit 7. Besides abundant *Clarkina wangi*, *Hindeodus julfensis* and *Iranognathus* sp. are also present in the entire zone. It roughly corresponds to the basal part of the *Hindeodus julfensis* Zone of IJRG (1981) (Fig. 11). IJRG (1981) also identified some *Clarkina orientalis* and *C. subcarinata* in this zone. Wang and Wang (1981) and Zhang (1987) split *C. wangi* from *C. subcarinata*, and Kozur (2005) established the new species *C. hambastensis* and the

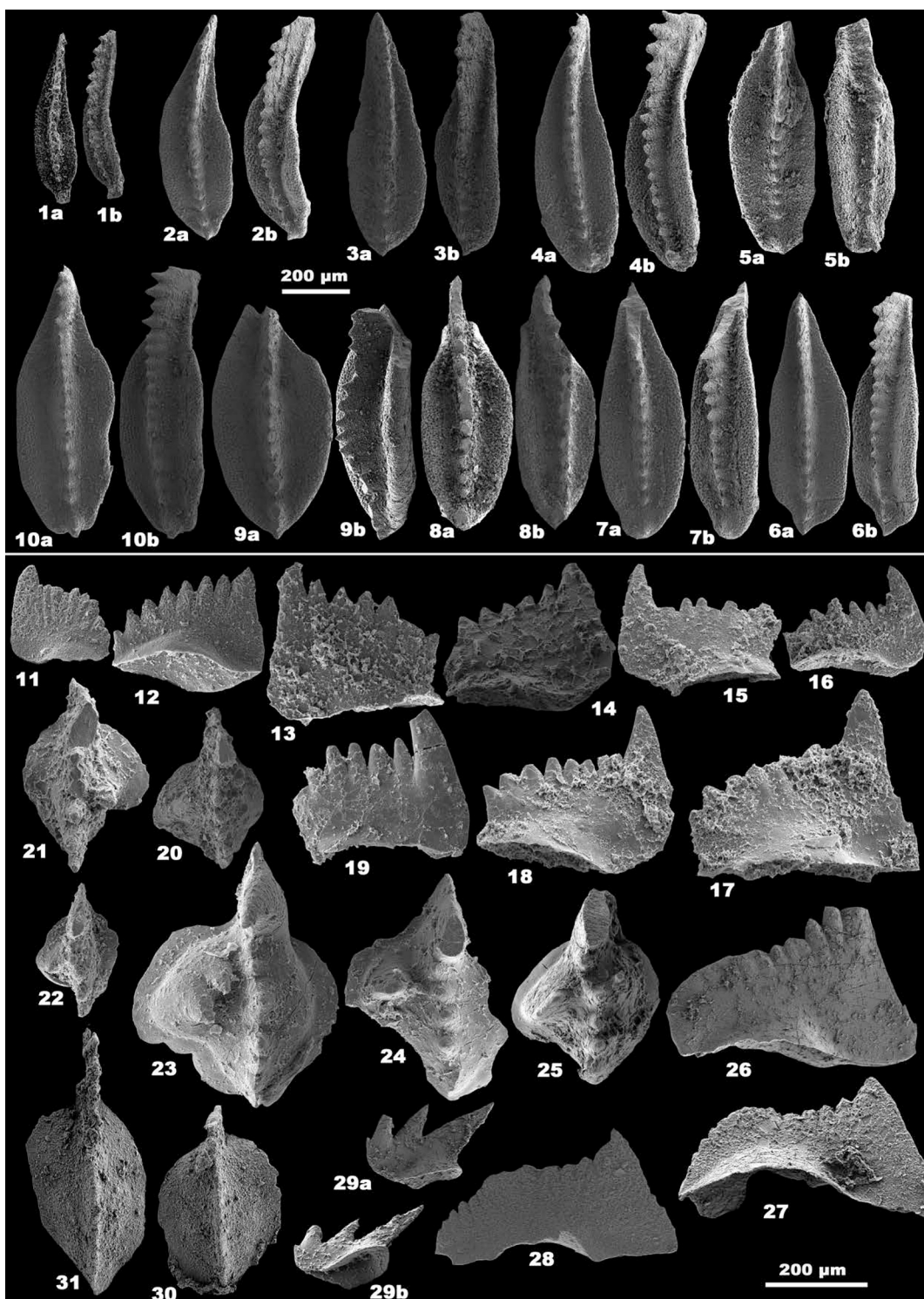


**Fig. 10.** 1–10. *Clarkina hauschkei*, from sample TEH -1.7 m. 11–14. *Hindeodus praeparvus*, 11 from sample TEH -1.5 m; 12, 13 from sample TEH -0.85~0.9 m; 14 from sample TEH -0.1~0.15 m. 15–19. *Hindeodus parvus*, from sample TEH -0.65~0.7 m. 20. *Isarcicella ?lobata*, from sample TEH 1.5 m. 21–24. *Isarcicella staeschei*, 21, 22 from sample TEH 1.5 m; 23, 24 from sample TEH 1.9~2.0 m. 25. *Isarcicella isarcica*, from sample TEH 1.9~2.0 m. 26–28. *Hindeodus julfensis*. 26 from sample TEH -36 m; 27 from sample ABS -6.65 m; 28 from sample TEH -4.75~4.76 m. 29. *Merrillina?divergens*, from sample TEH -36 m. 30, 31. *Iranognathus* sp., from sample TEH -21.9~22 m.

*C. hambastensis* Zone respectively in the same interval. *Clarkina hambastensis* was herein considered as a synonym of *C. wangi* (Shen and Mei, 2010; Yuan et al., 2014), and the two species even coexist in Sample 4a-2 at the Meishan section in South China (see Fig. 7 in Mei et al., 2004), which marks the base of the Changhsingian Stage. Therefore, the *C. wangi* Zone is adopted in this study. Kozur (2005) illustrated one

*C. longicupidata* within this zone, but its wall-like fused denticles on the carina suggest it is more similar to *C. hambastensis* (= *C. wangi*) rather than the typical *C. longicupidata*.

	Triassic Sys.	Induan Sta.	Elkah Fm.	Unit a	Conodont zones			
					IJRG, 1981	Kozur, 2004, 2005	Shen and Mei, 2010	This paper
Permian	Wuchiapingian	Hambast Fm.	Unit 7	Anchignathodus julfensis	<i>I. isarcica</i>	<i>Isarcicella isarcica</i>		<i>Isarcicella isarcica</i>
					<i>Anchignathodus parvus</i>	<i>Hindeodus parvus</i>		<i>I. staeschei</i>
					<i>M. ulti-S. ? most</i>			<i>Hindeodus parvus</i>
					<i>C. meish-H. praep</i>			<i>H. praeparvus</i>
					<i>C. hauschkei</i>			<i>C. hauschkei</i>
					<i>C. iranica</i>	<i>C. abadehensis</i>		<i>C. abadehensis</i>
					<i>C. zhangi</i>			<i>C. nodosa</i>
					<i>C. chang-C. defl</i>			<i>C. yini</i>
					<i>C. nodosa</i>			
					<i>C. bachmanni</i>	<i>C. changxingensis</i>		<i>C. changxingensis</i>
Abadeh Fm.	Unit 6	Gondolella orientalis	Clarkina orientalis	M. ulti-S. ? most = Merrillina ultima-Stepanovites ? mostleri	<i>C. subcarinata</i>	<i>C. subcarinata</i>		<i>C. subcarinata</i>
					<i>C. hambastensis</i>			<i>C. wangii</i>
					<i>C. longicuspidata</i>			<i>Clarkina orientalis</i>
					<i>Clarkina orientalis</i>			<i>Clarkina transcaucasica</i>
					<i>Clarkina transcaucasica</i>			<i>Clarkina transcaucasica</i>
					<i>Clarkina guangyuanensis</i>			
					<i>Clarkina leveni</i>			<i>Clarkina liangshanensis</i>
					<i>C. meish-H. praep</i> = <i>Clarkina meishanensis</i> - <i>Hindeodus praeparvus</i>			
					<i>C. chang-C. defl</i> = <i>C. changxingensis</i> - <i>Clarkina deflecta</i>			<i>Clarkina</i>

Fig. 11. Correlation of the conodont zones from different studies at the Abadeh section.

### 3.5. *Clarkina subcarinata* Zone (Sample TEH -5.75 m to TEH -4.75~4.76 m)

This zone is in the upper part of Unit 7. *Hindeodus* sp. and *Clarkina wangii* can be found in the basal part of the zone. IJRG (1981) figured one sample containing *C. subcarinata* and *C. orientalis* at the base of this zone. The range of *C. subcarinata* in Kozur (2005) is the same as this study. However, Kozur (2005) reported a sample with a few *C. bachmanni* at the uppermost part of this zone, which is inconsistent with our results, but cannot be re-evaluated because no specimen were illustrated. The *C. subcarinata* Zone was also recognized at the section in Shen and Mei (2010), but the base of the zone was uncertain in their study.

### 3.6. *Clarkina changxingensis* Zone (Sample TEH -4.75~-4.76 m to TEH -3.7 m)

This zone is in the upper part of Unit 7. *Hindeodus julfensis* and *Clarkina subcarinata* are found at the basal part of this zone. A few questionable *C. orientalis* and *C. subcarinata* were also reported in the lower part of the zone by IJRG (1981). One sample with *C. changxingensis* and *C. bachmanni* was figured at the basal part of this zone by Kozur (2005), indicating that the LO of *C. changxingensis* in Kozur (2004, 2005) is nearly consistent with this study. Therefore, we consider that it is more appropriate to establish the *C. changxingensis* Zone, which is globally adopted instead of the regional *C. bachmanni* Zone of Kozur (2005).

### 3.7. *Clarkina yini* Zone (Sample TEH -3.7 m to ABS -2.7 m)

This zone is in the upper part of Unit 7. One sample yielding *Hindeodus julfensis* at the basal part of this zone marks its highest occurrence (HO) at the Abadeh section, and two samples with specimens exhibiting more characters of *Clarkina changxingensis* also contain *C. yini*. The interval of *Clarkina yini* Zone in this study corresponds to the uppermost *C. bachmanni*, *C. nodosa* and *C. changxingensis*-*C. deflecta* zones in Kozur (2005) (Fig. 11). In fact, Kozur (2005) established the *C. nodosa* Zone at the Abadeh section based on a single sample, which was regarded as the top of its *C. nodosa* Zone, but no specimen of *C. nodosa* were found below and above the sample. Moreover, Kozur (2005) did not find *C. deflecta* in its *C. changxingensis*-*C. deflecta* Zone. Therefore, these zones are insufficiently defined at least at the Abadeh section by Kozur (2005). It is worth noting that the LO of *C. bachmanni* at the section coincides with the LO of *C. yini* in this study, and the two species can coexist throughout the *C. yini* Zone; whereas the LOs of *C. bachmanni* in Kozur (2005) are slightly lower or the same as the LOs of *C. changxingensis* at some sections in Iran. Shen and Mei (2010) also considered that *C. bachmanni* is a synonym of *C. yini*. In view of incongruent ranges and debatable taxonomy of *C. bachmanni*, the widely accepted *C. yini* Zone is used here. Furthermore, a few *Merrillina* sp. were found in the upper part of this interval by Kozur (2005).

### 3.8. *Clarkina nodosa* Zone (Sample ABS -2.7 m to ABS -1.9~2.0 m)

This zone is in the upper part of Unit 7. The lower part of this zone yielded abundant *Clarkina* specimens, including *C. nodosa* and *C. yini*, while its upper part yielded abundant *Hindeodus* specimens. The *Clarkina nodosa* Zone in this study corresponds to the *C. zhangi* Zone in Kozur (2005), which also reported a few *C. yini*, *C. deflecta* and *Merrillina* sp. Yuan et al. (2014) considered that *Clarkina zhangi* is a synonym of *C. yini*, and Shen and Mei (2010) suggested that the *C. nodosa* represents a geographic cline of *C. yini*. Therefore, most *Clarkina* in this interval found in Kozur (2004, 2005) likely belong to *C. yini*. In view of many *C. nodosa* and *C. yini* yielded in this interval, we consider that the *C. nodosa* Zone at the Abadeh section corresponds to the upper part of the *C. yini* Zone in South China.

### 3.9. *Clarkina abadehensis* Zone (Sample ABS -1.9~2.0 m to TEH -1.7 m)

This zone is in the top part of Unit 7. This zone yielded rare *Hindeodus* sp. Kozur (2005) originally named the interval as the *Clarkina iranica* Zone. Henderson et al. (2008) and Shen and Mei (2010) considered that *C. iranica* is a junior synonym of *C. abadehensis*, and the two species share the same ranges at many sections in Iran. We here agree with this opinion, and name this interval as the *C. abadehensis* Zone. *Clarkina abadehensis*, inferred to have evolved from *C. yini* in Iran, may correspond to the lower part of the *C. meishanensis* Zone according to the *C. abadehensis*-like specimens associated with *C. meishanensis* at Xifanli in South China (Shen and Mei, 2010). However, the LOs of *C. abadehensis* are lower than the LOs of probably *C. meishanensis* at many sections in Iran (Kozur, 2005). Therefore, further study is needed to clarify whether the *C. abadehensis* Zone corresponds to the uppermost *C. yini* Zone or the lower *C. meishanensis* Zone in South China.

### 3.10. *Clarkina hauschkei* Zone (Sample TEH -1.7 m to TEH -1.5 m)

This zone is in the topmost part of Unit 7. *Clarkina abadehensis* co-exists with *C. hauschkei* in our collections in the zone. Kozur (2004, 2005) also reported *C. abadehensis* in this interval, but did not find *C. hauschkei* at the section. Nevertheless, Kozur (2005) still established a *C. hauschkei* Zone above the *C. abadehensis* Zone at the section. Kozur (2004) illustrated a few *C. meishanensis* from the *C. hauschkei* Zone, and figured that the LOs of *C. meishanensis* are the same as *C. hauschkei* at some other sections in Iran. Moreover, *C. hauschkei* may be a junior synonym of *C. meishanensis* and could represent a geographic cline of *C. meishanensis* (Shen and Mei, 2010). Due to only one sample with rare *C. meishanensis* was found above the *C. hauschkei* Zone at the Abadeh section (Kozur, 2005), so we here still retain the *C. hauschkei* Zone. While Shen and Mei (2010) figured out that the *C. hauschkei* Zone in Iran corresponds to the upper part of the *C. meishanensis* Zone in South China, we suggest it may correspond to a part of *C. meishanensis* Zone.

### 3.11. *Hindeodus praeparvus* Zone (Sample TEH -1.5 m to TEH -0.65~0.7 m)

This zone is in the basal part of Unit a (Fig. 2B). The zone yielded many *Hindeodus*, but rare broken *Clarkina*. The LO of *Hindeodus praeparvus* in Kozur (2005) is slightly higher than this study, but the LO of its *Clarkina meishanensis* at the Abadeh section is consistent with the LO of *Hindeodus praeparvus* in this study (Fig. 3). Therefore, this indicates that the *H. praeparvus* Zone in this study corresponds to the *Clarkina meishanensis*-*Hindeodus praeparvus* Zone and the basal part of the *Merrillina ultima*-*Stepanovites*? *mostleri* Zone of Kozur (2005). Kozur (2004, 2005) also reported some *Hindeodus changxingensis* in the middle part of this interval. Moreover, the LO of *H. praeparvus* at the Meishan section in South China is lower than LOs of *H. changxingensis* and *Clarkina zhejiangensis* (Jiang et al., 2007; Zhang et al., 2009). It indicates that the

base of the *Hindeodus praeparvus* Zone in this study may be lower than the *H. changxingensis*- *Clarkina zhejiangensis* Zone at the Meishan section.

### 3.12. *Hindeodus parvus* Zone (Sample TEH -0.65~0.7 m to TEH 1.2 m)

This zone is also in the basal part of Unit a (Fig. 2B). Some *Hindeodus praeparvus* are present in the lower part of the zone. The LO of *H. parvus* at the Abadeh section in Kozur (2005) is higher than in this study, suggesting it roughly corresponds to the most part of the *Merrillina ultima*-*Stepanovites*? *mostleri* Zone and the *Hindeodus parvus* Zone of Kozur (2005). In addition, some *H. praeparvus*, *Clarkina zhejiangensis* and *Merrillina ultima* were reported in the *Merrillina ultima*-*Stepanovites*? *mostleri* Zone of Kozur (2005).

### 3.13. *Isarcicella staeschei* Zone (Sample TEH 1.2 m to TEH 1.9~2.0 m)

This zone is in the basal part of Unit a. This zone still contains many *Hindeodus parvus* and rare *Isarcicella*? *lobata*. One specimen illustrated as *I. staeschei* by Kozur (2004) is below the LO sample in this study, suggesting its level should be considered as the base of the *I. staeschei* Zone at the Abadeh section.

### 3.14. *Isarcicella isarcica* Zone (Sample TEH 1.9~2.0 m to unknown for its top)

This zone is in the lower part of Unit a. The top of this zone remains unclear because of no further samples were collected. The zone yielded *Hindeodus parvus*, *Isarcicella staeschei*, *I. isarcica* and *I. lobata*. Kozur (2004, 2005) did not find *I. isarcica* at the Abadeh section, but established the *I. isarcica* Zone based on the LO of *I. staeschei*. Therefore, it makes that the base of the zone in Kozur (2005) is lower than this study.

## 4. Discussion

### 4.1. The Guadalupian-Lopingian boundary

The GSSP for the Guadalupian-Lopingian boundary (GLB) was initially defined by the first appearance datum (FAD) of conodont *Clarkina postbitteri postbitteri* at the Penglaitan section in South China (Jin et al., 2006a). Recently, Shen et al. (2024) has redefined this GSSP at the new Penglaitan section by the FAD of *C. postbitteri*. *Clarkina postbitteri* is the first *Clarkina* species in its evolutionary lineage (Mei et al., 1994a; Henderson et al., 2002). Therefore, all strata containing *Clarkina* specimens around the GLB should be assigned to the Lopingian.

The GLB of the Abadeh section has never been precisely constrained since it was first described by Taraz (1969), and was first placed at the lithostratigraphic boundary between Units 4a and 4b, corresponding to the lower part of the Abadeh Formation. Taraz (1969) reported that Unit 4a mainly contains *Pachyphloia*, *Hemigordius* (=*Hemigordiopsis*), *Globivalvulina*, *Verbeekina*, *Chusenella*, and primitive *Codonofusiella*, which probably corresponds to the fusuline *Yabeina* Zone, and indicates a late Guadalupian age (Zhang and Wang, 2018). Two coral *Ipciphyllum* species, *I. simples* and *I. flexiosum* from Unit 3, which are common in the upper Maokou Formation in South China, further supports a late Guadalupian age (Shen et al., 2019b). IJRG (1981) subsequently updated the biostratigraphical data, and placed the GLB at the base of the large productid brachiopod *Araxilevis* Bed, which corresponds to the basal part of Unit 6. The topmost part of Unit 5 also contains *Araxilevis intermedius*, suggesting an early Lopingian age (Angiolini and Carabelli, 2010). More recently, Shahinfar et al. (2020) and Arefifard and Payne (2020) illustrated a few *Codonofusiella*, including a couple of *C. kwangsiensis* from the lower part of Unit 4b, which were used to reference the GLB in their papers. The ammonoid *Xenodiscus carbonarius* from the basal Unit 4b also suggests a Lopingian age, although *Xenodiscus* can span the GLB. It is also noteworthy that IJRG (1981) mentioned that one sample with *Chusenella* is about 60 m below the top

of Unit 4b, and Baghbani (1993) reported *Chusenella* in Unit 5. The highest occurrence (HO) of *Chusenella* is below the GLB (Zhang and Wang, 2018). Therefore, these age determinations by fusulines and ammonoids from Units 4b and 5 conflicts with each other.

Sweet and Mei (1999) suggested that the *Araxilevis* Bed and *Codonofusiella kwangsiana* Zone roughly corresponds to the conodont *Clarkina asymmetrica* Zone, and the horizon below the *Araxilevis* Bed is roughly assigned to the *Clarkina dukouensis* Zone. Shen and Mei (2010) followed this opinion and identified the base of Unit 6 representing the *Clarkina dukouensis* Zone, and they inferred that the top of Unit 5 may correspond to the unidentified *C. postbitteri* horizon. However, based on the specimens of *C. dukouensis* illustrated in their paper, this identification is problematic although the specimens show some characters of *C. dukouensis*. In this study, we found abundant typical *C. liangshanensis* and *C. ?guanyuanensis* in the upper part of Unit 5 (between -48.5 m and -36.6 m, Figs. 2A, 3), indicating that at least the upper part of Unit 5 should belong to the Wuchiapingian *C. liangshanensis* and *C. ?guanyuanensis* zones. We also found some reliable *Clarkina* in the lower part of Unit 5, which may also belong to the *C. liangshanensis* Zone. The lowest sample containing *Clarkina* specimens (Figs. 2A, 4.1) is at the basal part of Unit 5 (-75.1 m, Figs. 2A, 3), suggesting that the entire Unit 5 should be also assigned to Lopingian.

Moreover, multiple coquina beds consisting the possibly Guadalupian brachiopod *Permocryptospirifer* are present, and the highest one is at 54.3 m below the top of Unit 4b (-131.9 m, Fig. 2A) at the Abadeh section (Fig. 2G). This suggests that the GLB at the Abadeh section is likely below the lithological boundary between Units 4b and 5 and above the last coquina bed in Unit 4b, corresponding to the top part of Unit 4b, but precise GLB position within this interval cannot be identified because no age-indicative fossils were found.

The recent paper by Viaretti et al. (2025) located the GLB following Shen and Mei (2010) and Chen et al. (2020). However, the conodont zones (*Clarkina asymmetrica*, *C. leveni*, *C. guangyuanensis*) they reported for the lower part of Unit 6 (Fig. 1 in Viaretti et al., 2025) correspond to the *C. liangshanensis* Zone in the present paper, and the base of the *C. transcaucasica* Zone is in the same position, at 14 m from the base of Unit 6. The interpretation of climate warming at the base of the *C. transcaucasica* Zone remains valid (Viaretti et al., 2025).

#### 4.2. The Wuchiapingian-Changhsingian boundary

The GSSP for the Wuchiapingian-Changhsingian boundary (WCB) has been defined by the FAD of conodont *Clarkina wangii* at the Meishan D section in South China (Jin et al., 2006b). The Changhsingian was proposed as the last stage of the Lopingian based on its ammonoid fauna by Furnish and Glenister (1970) and Furnish (1973). Zhao et al. (1981) defined the base of the Changhsingian by the conodont succession between the *C. orientalis* and *C. subcarinata* zones, and *C. subcarinata* was subsequently used to recognize the basal Changhsingian (Wang and Wang, 1981; Jin et al., 1997). After *C. wangii* was named based on the primitive *C. subcarinata* with a wall-like fused carina, Mei et al. (2004) established the lineage *C. longicupidata*-*C. wangii*-*C. subcarinata*, which currently represents the interval around the WCB.

IJRG (1981) adopted the Dorashamian, proposed by Rostovtsev and Azaryan (1973) also based on its ammonoid fauna as the last stage of the Lopingian, and roughly placed the base of the Dorashamian at the boundary between Units 6 and 7. The ammonoid *Shevyrevites* Zone roughly indicates the base of the Dorashamian, but some *Shevyrevites* specimens were also reported from the upper part of Unit 6 (IJRG, 1981). *Paratirolites* species begin to occur in association with *Shevyrevites* from the middle part of Unit 7 at the section, and this interval was named the *Shevyrevites-Paratirolites* Zone or the *Paratirolites kittli* Sub-zone (Bando, 1979; IJRG, 1981). In South China, *Shevyrevites* and *Paratirolites* coexist in the top part of the Lungtan Formation at the Jiaozishan section in Guizhou (Zhao et al., 1981). The top part of the Lungtan Formation corresponds to the upper *Clarkina orientalis* Zone,

which is underlying the Changhsingian *C. wangii* Zone (Yuan et al., 2014, 2019; Shen et al., 2019b). The lower part of Unit 7 at the Abadeh section also belongs to the *Clarkina orientalis* Zone, as defined by IJRG (1981). Therefore, the WCB at the Abadeh section should be located above the lower part of Unit 7 and higher than the base of the traditional Dorashamian defined by ammonoids.

One sample with *Clarkina subcarinata* was figured from the middle part of Unit 7 at the Abadeh section by IJRG (1981). The specimen might represent primitive *C. subcarinata* (=*C. wangii*), which implies that this level lies around the WCB. However, this identification cannot be confirmed because no specimen was illustrated, and neither Kozur (2004, 2005) nor this study found *C. wangii* around this level. Kozur (2005) established *C. hambastensis* at the section, and defined the base of the Dorashamian by the LO of *C. hambastensis*. He considered that the LO of *C. hambastensis* is lower than that of *C. wangii*, and *C. hambastensis* is a transitional form between *C. longicupidata* and *C. wangii*. Based on our abundant conodonts from both Meishan and Abadeh sections, *C. hambastensis* is confirmed to be a synonym of *C. wangii*, and their ranges are correlative between the two sections. In addition, the specimen *C. longicupidata* illustrated by Kozur (2005) is more similar to *C. wangii* by having wall-like fused denticles on the carina rather than the typical *C. longicupidata*.

Based on the high-resolution conodont samples of this study, the LO of *Clarkina wangii* is slightly lower than the LO of *C. hambastensis* (=*C. wangii*) in Kozur (2005). Therefore, the WCB, also the base of the Dorashamian in Kozur (2005), is precisely constrained at 4.9 m below the top of the Hambast Formation at the Abadeh section.

#### 4.3. The Permian-Triassic boundary

The GSSP for the Permian-Triassic boundary (PTB) has been defined by the FAD of *Hindeodus parvus* at the Meishan D section in South China (Yin et al., 2001). Initially, the ammonoid *Otoceras* was used as the marker of the PTB. Yin et al. (1986) then proposed the conodont *Hindeodus parvus* as the marker to define the PTB. This definition made the *Otoceras* Zone to span the PTB, but the occurrences of abundant *Ophiceras* are also considered an auxiliary marker for identifying the PTB (Yin et al., 2001; Leonova, 2018; Yuan et al., 2019). Furthermore, although rare bivalve of the genus *Claraia* can be found at the topmost Permian, horizons with abundant *Claraia* are usually considered reliable indicators of an Early Triassic age.

The PTB interval at the Abadeh section has been intensively studied since Taraz (1969), but its precise level remains debated so far (e.g., Horacek et al., 2021; Chen et al., 2021; references herein). Due to rarity of fossils, Taraz (1969) placed the PTB at the lithostratigraphic boundary between Unit 7 and Unit a, noting the presence of many *Claraia* in the lower part of Unit a. IJRG (1981) reported a few *Hindeodus parvus* from the basal part of the Elikah Formation, and roughly put the PTB at the boundary between the Hambast and Elikah formations, marked by the boundary clay bed followed by a distinct microbialite unit. However, these *H. parvus* have never been illustrated. They also reported some *Ophiceras* and *Claraia* slightly above the microbialite unit with a calcite crystal fans. Gallet et al. (2000) mentioned *Hindeodus parvus* from the basal Elikah Formation but without illustration, and the level of their *Ophiceras* was not specified in detail. Kozur (2004, 2005) illustrated typical *Hindeodus parvus* from the top of the microbialite unit, and restricted the PTB to this level. Richoz et al. (2010) also illustrated some *Hindeodus parvus* from two samples, 94/264 and 94/265, in the basal part of the Elikah Formation. The level of Sample 94/264 was referred to as the PTB, but this sample yielded only a couple of broken *H. parvus*, which were later re-evaluated as a transitional form between *H. praeparvus* and *H. parvus* (see Chen et al., 2021 for details). Typical *H. parvus* was reported from Sample 94/265, which is in the upper part of the microbialite unit, slightly below the PTB of Kozur (2005). Our new data display numerous typical *H. parvus* specimens with a continuous range in this important interval, marking the LO of *H. parvus* at the

Abadeh section. This indicates that the PTB at this section is not higher than the middle part of the microbialite unit (Fig. 2B), similar to the results from the Dawen section, Great Bank of Guizhou, South China (Chen et al., 2009).

The topmost part of the Hambast Formation (~1 m below its top) at the Abadeh section still contains abundant Permian ammonoid *Paratirolites* (Bando, 1979; IJRG, 1981; Gallet et al., 2000). The changeover interval from *Clarkina*-dominated to *Hindeodus*-dominated is around the boundary clay (Fig. 2C) marked the base boundary of the Elikah Formation (Kozur, 2005; this study), which is slightly lower than the PTB at many sections in South China (Yuan et al., 2015, 2019). These might also indicate that the PTB at the section should be higher than the base of the Elikah Formation. Based on these observations, this study suggests that the precise PTB at the Abadeh section is at 0.8 m above the base of

the Elikah Formation (Fig. 2C).

In addition, the horizon of the PTB in the similar sequence at other sections in Iran and Armenia (e.g., Chanakhchi section) is also debated (Joachimski et al., 2020; Horacek et al., 2022, 2025; Han et al., 2025). Our results in this study could provide an important reference for these sections to identify the PTB.

## 5. Integrative Lopingian stratigraphic framework at the Abadeh section

Using the conodont biostratigraphical succession established above, an integrated high-resolution Lopingian stratigraphical framework, including lithostratigraphy, biostratigraphy, chemostratigraphy and magnetostratigraphy, is presented herein for global correlation

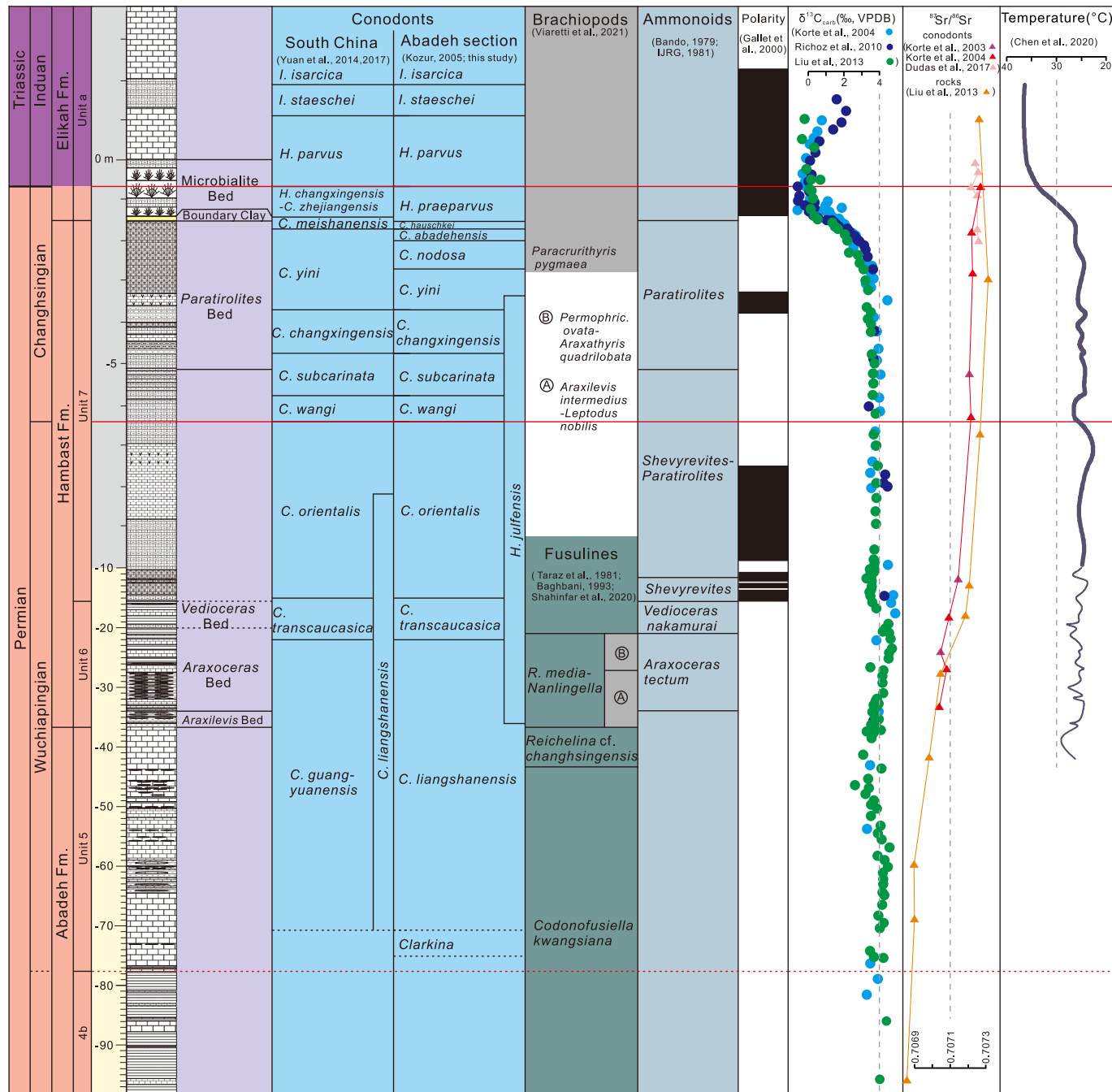


Fig. 12. Integrative stratigraphic framework of the Lopingian at the Abadeh section.

(Fig. 12).

### 5.1. Biostratigraphy

A wide variety of fossils, including conodonts, fusulines, ammonoids, and brachiopods, have been documented from the Abadeh section since it was described by Taraz (1969). Conodonts are currently the primary fossil group for subdivision and correlation of the Permian strata. The international Lopingian timescale has been established mainly based on the conodont succession from South China (Shen et al., 2010; Henderson and Shen, 2020). We here attempt to correlate all these fossil groups from Abadeh with the conodont succession of South China.

Reliable conodonts *Clarkina* indicating Lopingian begin to occur from the basal part of Unit 5 at the Abadeh section and become abundant in the upper part of Unit 5 (Figs. 2A, 3), and eleven conodont zones are recognized from the upper Wuchiapingian to the PTB at the section. The correlation between our new conodont zones and those in previous studies (IJRG, 1981; Kozur, 2004; Shen and Mei, 2010) has been discussed above (Fig. 11). Here, we briefly correlate our results with the conodont succession from South China. The *Clarkina liangshanensis* Zone represents the lowest Lopingian conodont zone at the Abadeh section at present. The *C. dukouensis* and *C. leveni* zones mentioned in previous studies are not adopted in this study. The *C. transcaucasica*, *C. orientalis*, *C. wangii*, *C. subcarinata* and *C. changxingensis* zones at Abadeh can be correlated directly with their counterparts in South China, and the *C. yini* and *C. nodosa* zones together are corresponding to the *C. yini* Zone in South China. *Clarkina abadehensis* correlates with the top part of the *C. yini* Zone and/or the lower part of the *C. meishanensis* Zone in South China, and the *C. hauschkei* Zone may correspond to a part of the *C. meishanensis* Zone. Due to rarity of *C. zhejiangensis* and *Hindeodus changxingensis* at Abadeh, we use the *H. praeparvus* Zone in this study, which corresponds to the topmost *Clarkina meishanensis* Zone and *H. changxingensis*-*Clarkina zhejiangensis* Zone. Although there is a minor inconsistency, the conodont succession between Abadeh and South China can be generally correlated in view of our new data.

Based on high-precision U—Pb ages and cyclostratigraphic data from South China, the durations of Lopingian conodont zones have been calculated for correlation (Yuan et al., 2019; Bagherpour et al., 2025). Due to the lack of direct age constraints, the durations of Changhsingian conodont zones in Abadeh were estimated using the PTB (Permian-Triassic boundary) and WCB (Wuchiapingian-Changhsingian boundary) ages from the international timescale. The estimated durations are as follows: *Clarkina wangii* (0.45 Myr), *C. subcarinata* (0.61 Myr), *C. changxingensis* (0.3 Myr), *C. yini* (0.54 Myr), *C. nodosa* (0.199 Myr), *C. abadehensis* (0.047 Myr), *C. hauschkei* (0.053 Myr), and *Hindeodus praeparvus* (0.039 Myr). It should be noted, however, that variable sedimentation rates at Abadeh may introduce significant uncertainties into these estimates.

IJRG (1981) established the fusuline *Sphaerulina*, *Codonofusiella kwangsiana* and *Reichelina media* zones in ascending order at the Abadeh section, corresponding to Unit 4, Unit 5 and most part of Unit 6, respectively. Baghbani (1993) and Shahinfar et al. (2020) subsequently added more data. Shahinfar et al. (2020) illustrated a few *Codonofusiella kwangsiana* from the lower part of Unit 4b, suggesting the base of the *C. kwangsiana* Zone is much lower than previously recognized. This zone has been widely regarded as the basal Wuchiapingian fusuline zone (e.g., Ueno and Tsutsumi, 2009; Ueno et al., 2010; Zhang and Wang, 2018). The Lopingian fusuline zones have been revised as the *Codonofusiella kwangsiana*, *Reichelina cf. changsingensis* and *R. media-Nanlingella* zones in ascending order (Fig. 12). The upper *Codonofusiella kwangsiana*, *Reichelina cf. changsingensis* and *R. media-Nanlingella* zones roughly correspond to the *Clarkina liangshanensis* Zone, which is of a Wuchiapingian age.

Early studies reported several ammonoid horizons from the Abadeh section (Taraz, 1969; Bando, 1979; IJRG, 1981). Bando (1979) simply figured *Xenodiscus* and *Cyclolobus* and established the *Araxoceras rotoides*

and *Shevyrevites shevyrevi* zones, which correspond to Units 6 and 7, respectively. The *Araxoceras rotoides* Zone contains two subzones, the *A. tectum* Subzone in the lower part and *Vedioceras nakamurai* Subzone in the upper part, and the *Shevyrevites shevyrevi* Zone includes the *S. shevyrevi* Subzone in the lower part and the *Paratirolites kittli* Subzone in the upper part. IJRG (1981) revised them as the *Araxoceras tectum*, *Vedioceras nakamurai*, *Shevyrevites*, *Shevyrevites-Paratirolites* and *Paratirolites* zones in ascending order (Fig. 12). In addition, Gallet et al. (2000) reported a horizon with *Paratirolites* at the topmost part of Unit 7, and Zakharov et al. (2010) added some new species in Unit 6, but the former ammonoid succession was not updated. In view of conodonts, the *Araxoceras tectum* Zone roughly corresponds to the topmost *Clarkina liangshanensis* Zone, the *Vedioceras nakamurai* Zone corresponds to the main part of the *C. transcaucasica* Zone, and the *Shevyrevites* Zone spans the boundary between the *C. transcaucasica* and *C. orientalis* zones. The *Shevyrevites-Paratirolites* Zone is equivalent to the interval from the basal part of the *C. orientalis* Zone to the middle part of *C. subcarinata* Zone, and the *Paratirolites* Zone is equivalent to the interval from the upper *C. subcarinata* Zone to the *C. hauschkei* Zone, respectively. It is noteworthy that Korn et al. (2021a, 2021b) reported many ammonoids and recognized more high-resolution Changhsingian ammonoid zones around the Baghuk Mountain. They concluded it is more likely that mixing of materials described by Bando (1979), and disagreed with some results of Bando (1979), IJRG (1981) and Zakharov et al. (2010) and consider that *Shevyrevites* cannot co-occur with *Paratirolites*, and *Araxoceras* cannot coexist with *Vedioceras*, respectively. Therefore, these discrepancies between the Hambast Range and Baghuk Mountain need further direct documents from the Abadeh sections to confirm.

Several Lopingian brachiopod horizons were also reported from the Abadeh section, but no brachiopod zone was established (Taraz, 1969; IJRG, 1981). Viaretti et al. (2021) re-collected brachiopod samples from the section, and established three assemblage zones, i.e., the *Araxilevis intermedius-Leptodus nobilis* and *Permophricodothyris ovata-Araxathyris quadrilobata* zones in Unit 6, and the *Paracrurithyris pygmaea* Zone at the top part of Unit 7. Our conodont succession constrains that the *Araxilevis intermedius-Leptodus nobilis* and *Permophricodothyris ovata-Araxathyris quadrilobata* zones correspond to the top part of the *Clarkina liangshanensis* Zone, and the *Paracrurithyris pygmaea* Zone is corresponding to the middle part of the *Clarkina yini* Zone, respectively. In addition, we found abundant possibly *Permocryptospirifer* shells in Unit 4b (Fig. 2G). *Permocryptospirifer* has been widely reported from South China and it ranges from the uppermost part of the Chihchia Formation to the middle-upper parts of the Maokou Formation, which generally indicates a Guadalupian age (Jin and Zhan, 2008). *Permocryptospirifer* usually disappeared in the upper part of the Guadalupian in South China (Capitanian), but never ranged upper into the topmost part of the Guadalupian in the world. Previously, Taraz (1974) reported *Permocryptospirifer iranica* from the middle part of Unit 3 (=Units 3 and 4a of IJRG, 1981), which is associated with the brachiopods *Richthofenia lawrenciana*, *Chnostegoides amernicus*, *Spinomarginifera helica*, *Leptodus* sp., *Orthothetina iljinae* (Nakamura and Golshani, 1981; IJRG, 1981). This suggests that the limestone unit containing abundant *Permocryptospirifer* found in this study is not the lowest occurrence of *Permocryptospirifer* and it is very likely of the upper Guadalupian.

### 5.2. Magnetostratigraphy

The paleomagnetic studies at the Abadeh section was carried out by Besse et al. (1998) and Gallet et al. (2000), which provided magnetostatigraphical data for the Hambast to Elikah formations. These data were later incorporated to establish the Lopingian geomagnetic polarity timescale by Hounslow and Balabanov (2018). Ten magnetic polarity intervals, including five normal and five reversal zones, were revealed within the Hambast Formation at Abadeh (Gallet et al., 2000). The lower four normals and the first three and a half reversals correspond to the Wuchiapingian (Fig. 12). The basal normal zone spans the boundary

between the *Clarkina transcaucasica* and *C. orientalis* zones, and the remaining Wuchiapingian magnetic polarity zones correspond to the *C. orientalis* Zone. The upper one normal zone and one and a half reversal zones belong to the Changhsingian. The upper part of the fourth reversal zone is corresponding to the *C. wangii*, *C. subcarinata* and *C. changxingensis* zones, while the fifth normal zone roughly corresponds to the lower *C. yini* Zone. The final Lopingian reversal zone encompasses the upper *C. yini*, *C. nodosa*, *C. abadehensis*, and *C. hauschkei* zones.

The magnetic polarity intervals in the Changhsingian at the Abadeh differ from those of the Meishan section in South China, where the polarity zones are predominantly normal, interspersed with five short reversals (Zhang et al., 2021). However, an important consistency between Abadeh and Meishan is that the *Clarkina yini* Zone roughly corresponds to the last Permian reversal, and all previous magnetostratigraphic studies in this region indicate that the Lower Triassic interval from the base *Hindeodus parvus* Zone is predominantly characterized by normal polarity, which could serve as a potential marker for global correlation (Besse et al., 1998; Gallet et al., 2000; Zhang et al., 2025a, 2025b). This polarity zone change is also consistent with the Shangsi section in South China, which could serve a potential marker for global correlation (Yuan et al., 2019). However, the high condensation of the Changhsingian Stage at Abadeh makes magnetostratigraphical work difficult.

### 5.3. Chemostratigraphy

High-resolution  $\delta^{13}\text{C}_{\text{carb}}$  chemostratigraphic data for the upper Guadalupian, through the Lopingian and across the PTB from eight sections in Iran and South China, including the Abadeh section, have been published (Korte et al., 2004; Richoz et al., 2010; Liu et al., 2013; Shen et al., 2013). We here compile a composite Lopingian  $\delta^{13}\text{C}_{\text{carb}}$  profile based on published data from the Abadeh section (Fig. 12). The composite profile shows a generally consistent trend from the GLB interval, through the Lopingian and across the PTB interval from these reference sections above. In view of our new conodont succession, the composite  $\delta^{13}\text{C}_{\text{carb}}$  profile extends from the GLB interval to the basal Triassic *Isarcicella staeschei* Zone. The  $\delta^{13}\text{C}_{\text{carb}}$  profile are relatively steady from the GLB interval and through the most part of the Lopingian followed by a progressively increased negative shift at the topmost part of the Changhsingian. There are three slight fluctuations, including two negative excursions and one positive excursion, below the lower part of the *Clarkina orientalis* Zone, which is relative to the average background value  $\sim 4\text{‰}$ .  $\delta^{13}\text{C}_{\text{carb}}$  value at the base of the profile in the GLB interval is  $\sim 4\text{‰}$ , and then displays the first negative fluctuation at the topmost part of Unit 4b. A gradually increase to over  $4\text{‰}$  at the basal *C. liangshanensis* Zone. The second negative shift of  $\sim 1\text{‰}$  is present in the middle *C. liangshanensis* Zone.  $\delta^{13}\text{C}_{\text{carb}}$  values subsequently recovered from around  $3\text{‰}$  to over  $4\text{‰}$  around the boundary between the *C. liangshanensis* and *C. transcaucasica* zones. A minor decline to the average background value in  $\delta^{13}\text{C}_{\text{carb}}$  is near the boundary between the *C. transcaucasica* and *C. orientalis* zones. The significance of these minor shifts in the Wuchiapingian for correlation needs to be evaluated based on other sections in different regions.

In the Changhsingian, the trend of  $\delta^{13}\text{C}_{\text{carb}}$  profile below the *Clarkina yini* Zone is still stable as it is in the Wuchiapingian *C. orientalis* Zone with some unobvious fluctuations, which is similar to many other sections in Iran and South China (Shen et al., 2013).  $\delta^{13}\text{C}_{\text{carb}}$  value progressively declined in the *C. yini* Zone at the section, followed by a sharp negative excursion to the lowest value of  $-0.5\text{‰}$  in the *Hindeodus praeparvus* Zone at the Abadeh section. The negative shift beginning from the *C. yini* Zone reached the lowest value  $\sim 5\text{‰}$  at the basal *H. praeparvus* Zone of the Elikah Formation. This large negative excursion has been widely regarded as the marker for the end-Permian mass extinction (EPME) (Korte and Kozur, 2010; Shen et al., 2013).  $\delta^{13}\text{C}_{\text{carb}}$  value began to increase in the *H. parvus* Zone, recovering to  $\sim 2\text{‰}$  in the *I. staeschei* Zone.

The strontium isotope ratio ( $^{87}\text{Sr}/^{86}\text{Sr}$ ) can also serve as an important chemostratigraphical tool (McArthur et al., 2012; Korte and Ullmann, 2018; Wang et al., 2018). The Lopingian  $^{87}\text{Sr}/^{86}\text{Sr}$  data from the Abadeh section have been reported by Korte et al. (2003, 2004), Liu et al. (2013) and Dudás et al. (2017). The  $^{87}\text{Sr}/^{86}\text{Sr}$  ratios in Korte et al. (2003, 2004) and Dudás et al. (2017) were measured using conodont apatite, while those in Liu et al. (2013) were obtained from bulk carbonate samples. Both datasets show similar  $^{87}\text{Sr}/^{86}\text{Sr}$  trends between the *Clarkina liangshanensis* Zone and the *Hindeodus parvus* Zone, but a distinct offset in  $^{87}\text{Sr}/^{86}\text{Sr}$  ratios is present between conodont and whole rock samples above the *Clarkina liangshanensis* Zone (Fig. 12).

The lowest  $^{87}\text{Sr}/^{86}\text{Sr}$  value between the upper Unit 4a and Unit 7 at the Abadeh section is 0.7068695, which may refer to the Capitanian minimum (Liu et al., 2013). The horizon of this data is located below the LO of *Clarkina* in our study (Fig. 12). In view of sampling intervals and  $^{87}\text{Sr}/^{86}\text{Sr}$  values, the real Capitanian minimum is possibly between Sample THE -66.8 m and THE -149 m. This deduction supports our conodont biostratigraphy that the GLB is possibly in the upper part of Unit 4b. In the Lopingian,  $^{87}\text{Sr}/^{86}\text{Sr}$  values rapidly increases to 0.7072083 based on whole rock samples in the middle *C. transcaucasica* Zone, and range from 0.707038 to 0.707092 between the top *C. liangshanensis* Zone and the middle *C. transcaucasica* Zone based on conodont samples. The  $^{87}\text{Sr}/^{86}\text{Sr}$  continues to increases to around 0.7073119 by carbonates and 0.707260 by conodonts from the *C. orientalis* Zone to the PTB interval, and doesn't display a significant signal around the PTB.

### 5.4. Correlation with other sections in Iran

Extensive stratigraphic studies of the Lopingian have been conducted in several other sections across central and northwestern Iran, including Shahreza, Baghuk Mountain, Kuh-e-Ali Bashi, and Zal (Teichert et al., 1973; Yazdi and Shirani, 2002; Partoazar, 2002; Korte et al., 2004; Kozur, 2004, 2005, 2007; Henderson et al., 2008; Shen and Mei, 2010; Heydari et al., 2013; Ghaderi et al., 2014; Leda et al., 2014; Isaa et al., 2016; Farshid et al., 2016; Korn et al., 2016, 2021a, 2021b). Regional correlation among these sections is crucial for reconstructing Iran's Lopingian timescale.

The Shahreza and Baghuk Mountain sections in central Iran exhibit stratigraphic sequences similar to those at Abadeh, with equivalent lithological units. Yazdi and Shirani (2002) documented a comparable conodont succession, including *Clarkina leveni*, *C. guangyuanensis*, *C. transcaucasica*, *C. orientalis*, and *C. subcarinata*, in both Shahreza and Abadeh. Although limited sample availability and stratigraphic resolution constrain precise dating, these findings suggest a depositional interval spanning the upper Wuchiapingian to lower Changhsingian. Korte et al. (2004) correlated the *C. leveni* and *C. transcaucasica* zones with most of Unit 6 and the uppermost Unit 6 to the lower part of Unit 7 in the Hambast Formation at Shahreza, respectively. Kozur (2004, 2005) further clarified that the *C. orientalis* Zone corresponds to the middle part of Unit 7, while all Changhsingian conodont zones align with its upper part, mirroring the succession at Abadeh. Farshid et al. (2016) and Korn et al. (2021a) identified eight Lopingian conodont zones in the upper Hambast Formation at Baghuk Mountain: the *C. orientalis*, *C. subcarinata*, *C. changxingensis*, *C. bachmanni*, *C. nodosa*, *C. yini*, *C. abadehensis*, and *C. hauschkei* zones in ascending order, consistent with those at Abadeh (Shen and Mei, 2010).

In contrast, the Kuh-e-Ali Bashi and Zal sections in northwestern Iran feature distinct stratigraphic sequences but remain broadly contemporaneous with central Iranian sections. The Lopingian timescale at Kuh-e-Ali Bashi has been contentious (see Henderson et al., 2008 for details). Based on materials from Sweet in Teichert et al. (1973), Shen and Mei (2010) recognized a complete Lopingian conodont succession at Kuh-e-Ali Bashi, correlating it with Abadeh, from the Wuchiapingian *Clarkina dukouensis* Zone at the base to the Changhsingian *C. hauschkei* Zone at the top. Subsequent studies (Ghaderi et al., 2014; Isaa et al., 2016) confirmed that central and northwestern Iranian sections share a similar

conodont succession, providing a robust framework for regional Lopingian correlation.

Ammonoid biostratigraphy further supports these correlations. Widely documented in both central and northwestern Iran, ammonoid sequences, including *Araxoceras*, *Vetriceras*, *Shevyrevites*, and *Paratirolites* beds in ascending order, offer additional stratigraphic ties (e.g., Teichert et al., 1973; IJRG, 1981). While Korn et al. (2021a, 2021b) questioned earlier Abadeh data, they presented a high-resolution ammonoid succession from Baghuk Mountain, proposing the following zones for central Iran: *Araxoceras*, *Pseudotoceras*, *Vetriceras*, *Dzhufites spinosus*, *Shevyrevites shevyrevi*, *S. nodosus*, *Paratirolites lanceolobatus*, *P. kittli*, *Alibashites ferdowsii*, *Al. profundus*, *Abichites abichi*, *Ab. stoyanowi*, and *Arasella minuta*. Ghaderi et al. (2014) and Korn et al. (2016) compiled analogous successions for Kuh-e-Ali Bashi and Zal. Although species-level discrepancies exist, genus-level consistency permits reliable Lopingian correlation between regions.

Chemostратigraphic data ( $\delta^{13}\text{C}_{\text{carb}}$ ) from Abadeh, Shahreza, Kuh-e-Ali Bashi, and Zal (Shen et al., 2013) reveal broadly synchronous trends. While minor Wuchiapingian  $\delta^{13}\text{C}_{\text{carb}}$  fluctuations vary slightly among sections, values consistently average  $\sim 4\text{‰}$ . A subtle decline occurs near the *C. orientalis* Zone, followed by a pronounced negative excursion between the *C. yini* and *Hindeodus parvus* zones. Korn et al. (2021a) reported a  $\delta^{13}\text{C}_{\text{carb}}$  profile from Baghuk Mountain (upper Wuchiapingian to basal Triassic), matching patterns in Shen et al. (2013). However, they placed the onset of the negative trend in the *C. changxingensis* Zone, slightly lower than other sections. In reality, the major excursion ( $\delta^{13}\text{C}_{\text{carb}} < 3\text{‰}$ ) begins in their *C. nodosa* Zone, which overlaps with part of the *C. yini* Zone in our updated conodont succession.

## **6. No distinct end-Guadalupian mass extinctions at the Abadeh section**

The end-Guadalupian mass extinction (EGME) has been debated as a potential distinct event since its initial recognition (Jin et al., 1994;

Stanley and Yang, 1994). While studies propose various causes, such as marine regression, Emeishan volcanism, and oceanic anoxia (Wignall et al., 2009; He et al., 2010; Song et al., 2023), the fossil-based definition of the EGME remains ambiguous. Recent analyses suggest the EGME may reflect a gradual biodiversity decline or episodic turnovers spanning the Wordian to Wuchiapingian (Shi and Yang, 2005; Clapham et al., 2009; Groves and Wang, 2013; Zhang et al., 2025a, 2025b), rather than a discrete short event (Fan et al., 2020; Shen et al., 2020).

At the Abadeh section, despite a continuous GLB interval, no distinct EGME marker is observed around the GLB interval (Fig. 13). Although Shahinfar et al. (2020) identified the GLB via the fusuline *Codonofusilliella kwangsiana* in lower Unit 4b, and Arefifard and Payne (2020) interpreted depositional changes across Units 4a-4b, these studies do not suggest a rapid extinction. Compiled data reveal that 60 % (77 of 120) of species with lowest occurrences (LOs) below the GLB disappeared within the GLB interval (Fig. 13). However, this decline spanned nearly the entirety of Unit 4, displaying a prolonged and gradual pattern rather than an abrupt mass extinction. Highest occurrences (HOs) further indicate that Guadalupian fauna persisted until the middle Wuchiapingian, with no concentrated extinction horizon. Thus, the Abadeh section supports a model of protracted ecological turnover rather than a distinct end-Guadalupian extinction event.

Chemostratigraphy across the GLB interval (Fig. 12) does not show any major  $\delta^{13}\text{C}_{\text{carb}}$  excursion as reported from other areas (e.g., South China, North America) (Wignall et al., 2009; Shen et al., 2013, 2020). This probably suggests that the sharp negative  $\delta^{13}\text{C}_{\text{carb}}$  excursion found around the GLB section in South China may be due to the unconformity and organic burial in the Wangpo Shale related to the initial transgression (Shen et al., 2013). Whereas the Penglaitan section in South China with a continuous deposition around GLB suggests no major  $\delta^{13}\text{C}_{\text{carb}}$  excursion as well (Chen et al., 2013), which is consistent with the Abadeh section.

Liu et al. (2013) reported a minor negative depletion in association with a low value of 0.7069 of  $^{87}\text{Sr}/^{86}\text{Sr}$  ratio. However, our newly found conodonts indicate this minor excursion is still within the

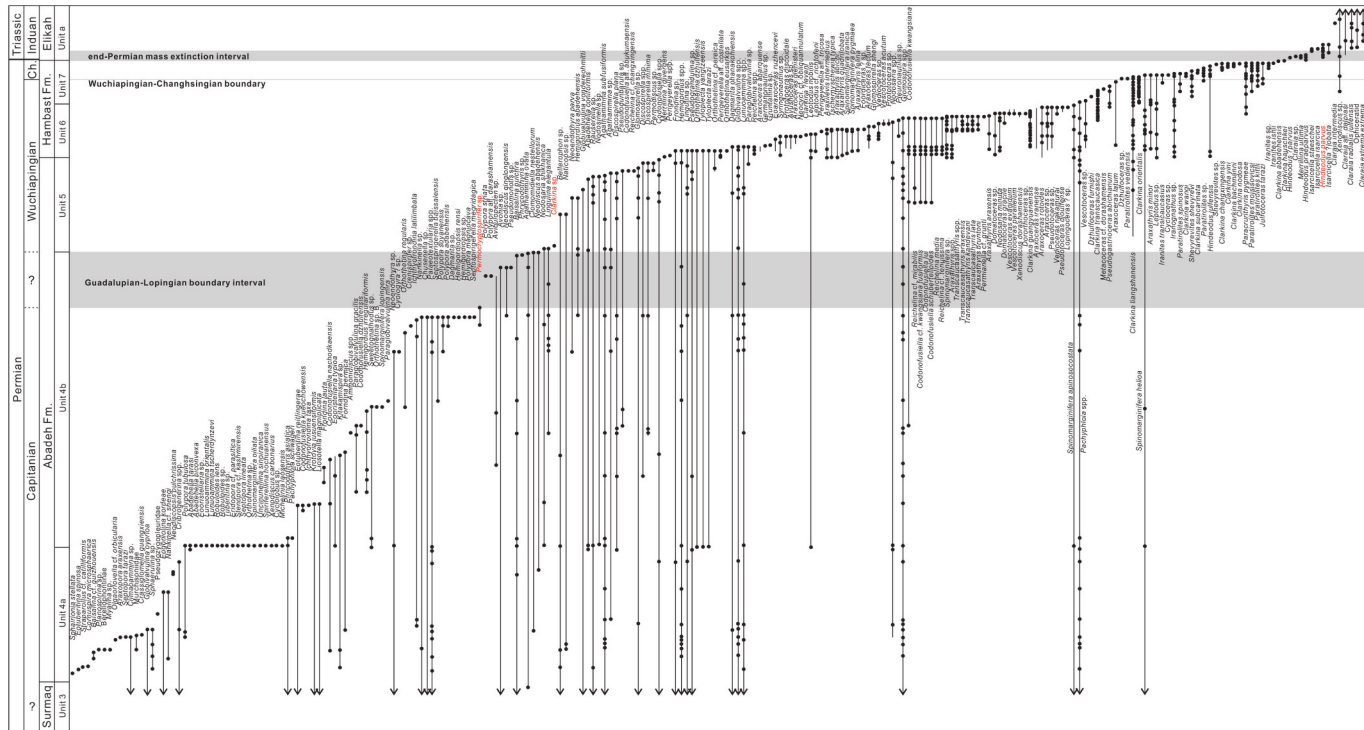


**Fig. 13.** Fossil records from the late Guadalupian to the Early Triassic at the Abadeh section (data from IJRG, 1981; Kozur, 2005; Gallet et al., 2000; Zakharov et al., 2010; Shahinfar et al., 2020; Viaretti et al., 2021; this study).

Wuchiapingian and  $^{87}\text{Sr}/^{86}\text{Sr}$  ratio remains steadily low from the uppermost Guadalupian to the lowest Wuchiapingian. Another minor negative shift is present at the base of Unit 5 (-77.6 m), which may be a potential marker for the GLB.  $^{87}\text{Sr}/^{86}\text{Sr}$  ratio also generally supports that the GLB is within this interval as mentioned above.

## 7. End-Permian mass extinction at the Abadeh section

The Abadeh section showed a different biological extinction pattern around the PTB based on all recorded fossil ranges (Fig. 13). Our compilation data show that over 98 % (136 of 138) of Permian species above the GLB interval disappeared below the boundary clay, which marks the onset of the end-Permian mass extinction (EPME) at the Abadeh section (Shen et al., 2013). Actually, more than 98 % (136 of 138) of Permian species above the GLB interval disappeared below the boundary clay, mostly in the Wuchiapingian because the Changhsingian Stage at the Abadeh section is highly condensed in the top (Fig. 13). This pattern is in contrast to the sudden pattern at the Meishan section in South China where a large part of the Permian taxa disappeared within the Changhsingian just below the PTB (Jin et al., 2000; Shen et al., 2011, 2019a; Song et al., 2013; Wang et al., 2014). We interpret that this is because the depositional setting at Abadeh from the upper Wuchiapingian shifted to a pelagic environment in the Changhsingian (Kozur, 2004, 2005) where benthic fossils may not be diverse in the pelagic habitat areas. This change resulted in the disappearances of many benthic fossils prevailed in the Wuchiapingian and dominance of the pelagic nektonic conodonts and ammonoids in the Changhsingian.

Nonetheless, some distinct community changes around the EPME have been observed at the Abadeh section. However, it is important to note that conodonts, as a group with inherently high turnover rates, may reflect evolutionary transitions rather than true extinction signals. First, the conodont community shows a distinct change at the boundary clay, shifting from extremely abundant *Clarkina*-dominated assemblages below to *Hindeodus*- and *Isarcicella*-dominated communities above. While this faunal turnover parallels patterns observed in South China (e.g., Yuan et al., 2015, 2019), its interpretation as a mass extinction signal requires caution given conodonts' natural turnover characteristics. Second, the unit with the distinct ammonoid assemblage dominated by the *Paratirolites* ended at the boundary clay, replaced above by abundant bivalves and smooth ammonoids (e.g., *Claraia*, *Ophiceras*). This transition may be more informative for extinction studies, as ammonoids typically have lower background turnover rates than conodonts. Furthermore, we recognize that depositional environment changes (particularly the shift to deeper water facies) may have significantly influenced fossil preservation and our ability to detect extinction patterns across the boundary interval.

In addition to the fossil changes, the distinct fan-like microbialite unit strongly suggest the EPME at the Abadeh section. This microbialite unit has been widely observed globally across the Permian-Triassic extinction interval (Chen et al., 2009; Kershaw et al., 2012; Zheng et al., 2016; Foster et al., 2020; Heuer et al., 2022; Han et al., 2025).

$\delta^{13}\text{C}_{\text{carb}}$  isotope chemostratigraphy (Korte et al., 2004; Horacek et al., 2007; Richoz et al., 2010; Shen et al., 2013) show a basically consistent trend with that at the Meishan section and many other sections. It shows a progressive gradual decline with a magnitude of ~4 ‰ that started from the middle of the *Clarkina yini* Zone and reached the lowest point in the *Hindeodus praeparvus* Zone.  $\delta^{18}\text{O}_{\text{apatite}}$  values are relatively stable, fluctuating in the range of 18.28–20.15 ‰ with an average of 19.44 ‰ below the EPME interval (Fig. 12; Chen et al., 2020). A sudden decrease occurs in the *Clarkina hauschkei* Zone and reaches a low value of 17.05 ‰ close to the PTB, which indicates a rapid warming event of ~10 °C above the onset of the EPME and below the PTB at Abadeh. This paleotemperature change is completely consistent with that at the Meishan section (Joachimski et al., 2012; Chen et al., 2016).

Overall, the Abadeh section displayed a consistent EPME pattern with that in other regions, but most of the fossil ranges disappeared

much below the Changhsingian Stage which is probably resulted from the changes of lithofacies reflecting a Signor-Lipps effect.

## 8. Conclusions

Based on more than 200 conodont samples, this study for the first time presents a high-resolution Lopingian conodont succession at the Abadeh section. Fourteen conodont zones have been recognized from the middle Abadeh Formation to the basal Elikah Formation, and they are the *Clarkina liangshanensis*, *C. transcaucasica*, *C. orientalis*, *C. wangi*, *C. subcarinata*, *C. changxingensis*, *C. yini*, *C. nodosa*, *C. abadehensis*, *C. hauschkei*, *Hindeodus praeparvus*, *H. parvus*, *Isarcicella staeschei* and *I. isarcica* zones in ascending order, which can be well correlated with the international standard from South China.

Our new conodont biostratigraphy at Abadeh suggests that the Guadalupian-Lopingian boundary (GLB) is below Unit 5 and possibly within Unit 4b based on the lowest occurrence (LO) of reliable *Clarkina* conodonts at the base of Unit 5. The Wuchiapingian-Changhsingian boundary (WCB) is indicated by the LO of *C. wangi* at 4.9 m below the top of the Hambast Formation. The Permian-Triassic boundary (PTB) is at 0.8 m above the base of the Elikah Formation, based on the LO of the characteristic *Hindeodus parvus*.

A high-resolution regional timescale for the Lopingian is integrated based on lithostratigraphical, biostratigraphical, chemostratigraphical and magnetostratigraphical data from the Abadeh sections. This integrative timescale based on the Abadeh section in central Iran provides the most precise temporal framework for both regional and global correlation of the Lopingian and the PTB interval.

An integrated fossil record including foraminifera, corals, brachiopods, bivalves, ammonoids and conodonts from the Abadeh sections is compiled. It indicates that over 60 % of Guadalupian species disappeared below the GLB interval, but no distinct mass extinction interval was identified. No major chemostratigraphical signals are detected around the GLB interval at the Abadeh section.

On the other hand, the EPME is basically consistent with all other sections in the world as indicated by a major negative  $\delta^{13}\text{C}_{\text{carb}}$  excursion of ~4 ‰ starting from the *Clarkina yini* Zone. This is also supported by the  $\delta^{18}\text{O}_{\text{apatite}}$  excursion just below the PTB indicating an abrupt ~10 °C temperature rise. The massive disappearances of many benthic fossils below the Changhsingian at the Abadeh section is clearly a Signor-Lipps effect. The EPME is well displayed at the boundary clay by the sudden occurrence of fan-like microbialite unit, the changeover from the *Clarkina-Paratirolites*-dominated to the *Hindeodus-Ophiceras-Claraia*-dominated communities.

## CRediT authorship contribution statement

**Dong-xun Yuan:** Writing – original draft, Investigation, Funding acquisition, Conceptualization. **Yi-chun Zhang:** Writing – review & editing, Investigation. **Mohammad N. Gorgij:** Writing – review & editing, Investigation, Funding acquisition. **Hua Zhang:** Writing – review & editing, Investigation. **Lucia Angiolini:** Writing – review & editing, Investigation. **Gaia Crippa:** Writing – review & editing, Investigation. **Jun Chen:** Writing – review & editing. **Shu-zhong Shen:** Writing – review & editing, Supervision, Investigation, Funding acquisition.

## Declaration of competing interest

The authors declare that they have no known competing financial interests or personal relationships that could have appeared to influence the work reported in this paper.

## Acknowledgements

We thank William Foster, Borhan Bagherpour, two other anonymous

reviewers and editors for their helpful comments to improve the manuscript. We also thank Prof. Wei Wang and Qiong Wu for their suggestions and help during fieldwork. This work is supported by the National Natural Science Foundation of China (NSFC) (42272031, 42261144668, 42072013), and Jiangsu Innovation Support Plan for International Science and Technology Cooperation Program (BZ2023068). MNG is supported by the common project between China and Iran of Iran National Science Foundation (INSF) (4006320).

## Data availability

No data was used for the research described in the article.

## References

- Algeo, T.J., Shen, J., 2024. Theory and classification of mass extinction causation. *Natl. Sci. Rev.* 11, nwad237.
- Angiolini, L., Carabelli, L., 2010. Upper Permian brachiopods from the Nesen Formation, North Iran. *Spec. Pap. Palaeontol.* 84, 41–90.
- Angiolini, L., Checconi, A., Gaetani, M., Rettori, R., 2010. The latest Permian mass extinction in the Alborz Mountains (North Iran). *Geol. J.* 45, 216–229.
- Angiolini, L., Crippa, G., Shen, S.Z., Zhang, H., Zhang, Y.C., Ghorbani, M., Ghorbani, M., Ovissi, M., 2017. Report of the Chinese, Italian, Iranian working group: the Permian-Triassic boundary sections of Abadeh revisited. *Permophiles* 65, 24–27.
- Arefifard, S., Baud, A., 2022. Depositional environment and sequence stratigraphy architecture of continuous Upper Permian and Lowermost Triassic deep marine deposits in NW and SW Iran. *Palaeogeogr. Palaeoclimatol. Palaeoecol.* 603, 111187.
- Arefifard, S., Payne, J.L., 2020. End-Guadalupian extinction of larger fusulinids in Central Iran and implications for the global biotic crisis. *Palaeogeogr. Palaeoclimatol. Palaeoecol.* 550, 109743.
- Baghbani, D., 1993. The Permian Sequence in the Abadeh Region, Central Iran. Occasional Publication, Earth Sciences and Resources Institute, University of South Carolina, New Series, B, 9, pp. 7–22.
- Bagherpour, B., De Lena, L.F., Ovtcharova, M., Yuan, D.X., Shen, S.Z., Bucher, H., Schaltegger, U., 2025. Correlating early Wuchiapingian (early Lopingian/late Permian) biotic and environmental changes with eruptive activity of the Emeishan LIP. *Lithos* 494–495, 107937.
- Bando, Y., 1979. Upper Permian and Lower Triassic Ammonoids From Abadeh, Central Iran. Memoirs of the Faculty of Education, Kagawa University, 29, pp. 103–138.
- Besse, J., Torcq, F., Gallet, Y., Ricou, L.E., Krystyn, L., Saidi, A., 1998. Late Permian to Late Triassic palaeomagnetic data from Iran: constraints on the migration of the Iranian block through the Tethyan Ocean and initial destruction of Pangaea. *Geophys. J. Int.* 135, 77–92.
- Chen, J., Shen, S.Z., 2019. Mid-Permian (End-Guadalupian) extinctions. In: Reference Module in Earth Systems and Environmental Sciences. Elsevier, pp. 1–8.
- Chen, J., Xu, Y.G., 2019. Establishing the link between Permian volcanism and biodiversity changes: Insights from geochemical proxies. *Gondw. Res.* 75, 68–96.
- Chen, J., Beatty, T.W., Henderson, C.M., Rowe, H., 2009. Conodont biostratigraphy across the Permian-Triassic boundary at the Dawen section, Great Bank of Guizhou, Guizhou Province, South China: Implications for the Late Permian extinction and correlation with Meishan. *J. Asian Earth Sci.* 36, 442–458.
- Chen, B., Joachimski, M.M., Shen, S.Z., Lambert, L.L., Lai, X.L., Wang, X.D., Chen, J., Yuan, D.X., 2013. Permian ice volume and palaeoclimate history: Oxygen isotope proxies revisited. *Gondw. Res.* 24, 77–89.
- Chen, J., Shen, S.Z., Li, X.L., Xu, Y.G., Joachimski, M.M., Bowring, S.A., Erwin, D.H., Yuan, D.X., Chen, B., Zhang, H., 2016. High-resolution SIMS oxygen isotope analysis on conodont apatite from South China and implications for the end-Permian mass extinction. *Palaeogeogr. Palaeoclimatol. Palaeoecol.* 448, 26–38.
- Chen, J., Shen, S.Z., Zhang, Y.C., Angiolini, L., Gorgij, M.N., Crippa, G., Wang, W., Zhang, H., Yuan, D.X., Li, X.H., Xu, Y.G., 2020. Abrupt warming in the latest Permian detected using high-resolution *in situ* Oxygen isotopes of conodont apatite from Abadeh, Central Iran. *Palaeogeogr. Palaeoclimatol. Palaeoecol.* 560, 109973.
- Chen, J., Yuan, D.X., Shen, S.Z., 2021. Reply to the Comment of Horacek et al. (2021) on the Permian-Triassic boundary at the Abadeh section, central Iran. *Permophiles* 71, 39–43.
- Clapham, M.E., Shen, S.Z., Bottjer, D.J., 2009. The double mass extinction revisited: reassessing the severity, selectivity, and causes of the end-Guadalupian biotic crisis (Late Permian). *Paleobiology* 35, 32–50.
- Dudás, F.Ö., Yuan, D.X., Shen, S.Z., Bowring, S.A., 2017. A conodont-based revision of the  $^{87}\text{Sr}/^{86}\text{Sr}$  seawater curve across the Permian-Triassic boundary. *Palaeogeogr. Palaeoclimatol. Palaeoecol.* 470, 40–53.
- Erwin, D.H., 1990. The end-Permian mass extinction. *Annu. Rev. Ecol. Syst.* 21, 69–91.
- Fan, J.X., Shen, S.Z., Erwin, D.H., Sadler, P.M., MacLeod, N., Cheng, Q.M., Hou, X.D., Yang, J., Wang, X.D., Wang, Y., Zhang, H., Chen, X., Li, G.X., Zhang, Y.C., Shi, Y.K., Yuan, D.X., Chen, Q., Zhang, L.N., Li, C., Zhao, Y.Y., 2020. A high-resolution summary of Cambrian to Early Triassic marine invertebrate biodiversity. *Science* 367, 272–277.
- Farshid, E., Hamdi, B., Hairapetian, V., Aghanabati, S.A., 2016. Conodont biostratigraphy of the Permian-Triassic boundary in the Baghuk mountain section Northwest of Abadeh. *Geosciences* 25, 285–294.
- Foster, W.J., Heindel, K., Richoz, S., Gliwa, J., Lehrmann, D.J., Baud, A., Kolar-Jurkovsek, T., Aljinovic, D., Jurkovsek, B., Korn, D., Martindale, R.C., Peckmann, J., 2020. Suppressed competitive exclusion enabled the proliferation of Permian/Triassic boundary microbialsites. *Depositional Rec.* 6, 62–74.
- Furnish, W.M., 1973. Permian stage names. *Can. Soc. Petrol. Geol. Mem.* 2, 522–548.
- Furnish, W.M., Glenister, B.F., 1970. Permian ammonoid *Cyclolobus* from the Salt Range, West Pakistan. In: Kummel, B., Teichert, G. (Eds.), *Stratigraphic Boundary Problems, Permian and Triassic of West Pakistan*, 4. Kansas University, Department of Geology, Special Publication, pp. 153–175.
- Gallet, Y., Krystyn, L., Besse, J., Saidi, A., Ricou, L.E., 2000. New constraints on the Upper Permian and lower Triassic geomagnetic polarity timescale from the Abadeh section (Central Iran). *J. Geophys. Res. Solid Earth* 105 (B2), 2805–2815.
- Ghaderi, A., Leda, L., Schobben, M., Korn, D., Ashouri, A.R., 2014. High-resolution stratigraphy of the Changhsingian (Late Permian) successions of NW Iran and the Transcaucasus based on lithological features, conodonts and ammonoids. *Fossil Rec.* 17, 41–57.
- Glenister, B.F., Furnish, W.M., 1961. The Permian ammonoids of Australia. *J. Paleo.* 35, 673–736.
- Groves, J.R., Wang, Y., 2013. Timing and size Selectivity of the Guadalupian (Middle Permian) Fusulinoidean Extinction. *J. Paleo.* 87, 183–196.
- Gullo, M., Kozur, H.W., 1992. Conodonts from the pelagic deep-water Permian of central western Sicily (Italy). *Neues Jahrbuch für Geologie und Paläontologie* 184, 203–234.
- Han, C., Wu, S.L., Zhao, H., Lyu, Z.Y., Mei, Q.Y., Zhao, L.S., 2025. Uppermost Permian to lower Triassic conodont biostratigraphy and carbon isotope records from Southern Armenia. *Palaeogeogr. Palaeoclimatol. Palaeoecol.* 667, 112870.
- He, B., Xu, Y.G., Zhong, Y.T., Guan, J.P., 2010. The Guadalupian-Lopingian boundary mudstones at Chaotian (SW China) are clastic rocks rather than acidic tuffs: Implication for a temporal coincidence between the end-Guadalupian mass extinction and the Emeishan volcanism. *Lithos* 119, 10–19.
- Henderson, C.M., Shen, S.Z., 2020. Chapter 24—the Permian Period. In: Gradstein, F.M., Ogg, J.G., Schmitz, M.D., Ogg, G.M. (Eds.), *The Geologic Time Scale 2020*. Elsevier, pp. 875–902.
- Henderson, C.M., Mei, S.L., Wardlaw, B.R., 2002. New conodont definitions at the Guadalupian-Lopingian Boundary. In: Hills, L.V., Henderson, C.M., Bamber, E.M. (Eds.), *Carboniferous and Permian of the World*. Canadian Society of Petroleum Geologists Memoir, 19, pp. 725–735.
- Henderson, C.M., Mei, S.L., Shen, S.Z., Wardlaw, B.R., 2008. Resolution of the reported Upper Permian conodont occurrences from northwestern Iran. *Permophiles* 51, 2–9.
- Heuer, F., Leda, L., Moradi-Salimi, H., Gliwa, J., Hairapetian, V., Korn, D., 2022. The Permian-Triassic boundary section at Baghuk Mountain, Central Iran: carbonate microfacies and depositional environment. *Palaeobiodivers. Palaeoenviron.* 102, 331–350.
- Heydari, E., Arzani, N., Safaei, M., Hassanzadeh, J., 2013. Ocean's response to a changing climate: Clues from variations in carbonate mineralogy across the Permian-Triassic boundary of the Shareza Section, Iran. *Global Planet. Change* 105, 79–90.
- Horacek, M., Brandner, R., Abart, R., 2007. Carbon isotope record of the P/T boundary and the lower Triassic in the Southern Alps: evidence for rapid changes in storage of organic carbon. *Palaeogeogr. Palaeoclimatol. Palaeoecol.* 252, 347–354.
- Horacek, M., Krystyn, L., Baud, A., 2021. Comment to Chen et al., 2020: abrupt warming in the latest Permian detected using high-resolution *in situ* oxygen isotopes of conodont apatite from Abadeh, Central Iran: importance of correct stratigraphic correlation, reporting of existing data and their scientific interpretation. Importance of correct stratigraphic correlation, reporting of existing data and their scientific interpretation. *Permophiles* 70, 33–36.
- Horacek, M., Krystyn, L., Baud, A., 2022. Siberian Trap volcanism, global warming and the Permian-Triassic mass extinction: New insights from Armenian Permian-Triassic sections: Comment. *Geol. Soc. Am. Bull.* 134, 1085–1086.
- Horacek, M., Zakharov, Y., Krystyn, L., Baud, A., Grigoryan, A., 2025. Comment on "Uppermost Permian to lower Triassic conodont biostratigraphy and carbon isotope records from Southern Armenia". *Palaeogeogr. Palaeoclimatol. Palaeoecol.* 668, 112912.
- Hounslow, M.W., Balabanov, Y.P., 2018. A geomagnetic polarity timescale for the Permian, calibrated to stage boundaries. In: Lucas, S.G., Shen, S.Z. (Eds.), *The Permian Timescale*. Geol. Soc. Lond. Spec. Publ. 450, 61–103.
- Iranian-Japanese Research Group, 1981. The Permian and the Lower Triassic Systems in Abadeh Region, Central Iran. Memoirs of the Faculty of Science, Kyoto University, Series of Geology and Mineralogy, 47, pp. 61–133.
- Isaa, A., Ghaderi, A., Ashouri, A.R., Korn, D., 2016. Late Permian Early Triassic conodonts of the Zal section at the northwest of Iran. *J. Stratigr. Sedimentol. Res.* 32, 55–57.
- Jiang, H.S., Lai, X.L., Luo, G.M., Aldridge, R.A., Zhang, K.X., Wignall, P.B., 2007. Restudy of conodont zonation and evolution across the P/T boundary at Meishan section, Changxing, Zhejiang, China, environmental and biotic changes during the Paleozoic-Mesozoic transition. *Global Planet. Change* 55, 39–55.
- Jin, X.C., Zhan, L.P., 2008. Spatial and temporal distribution of the *Cryptospirifer* fauna (Middle Permian brachiopods) in the Tethyan realm and its paleogeographic implications. *Acta Geol. Sin.* 1, 1–16.
- Jin, Y.G., Zhang, J., Shang, Q.H., 1994. Two phases of the end-Permian mass extinction. In: Embry, A.F., Beauchamp, B., Glass, D.J. (Eds.), *Canadian Society of Petroleum Geologists Memoir*, 17, pp. 813–822.
- Jin, Y.G., Wardlaw, B.R., Glenister, B.F., Kotlyar, C.V., 1997. Permian chronostratigraphic subdivisions. *Episodes* 20, 6–10.
- Jin, Y.G., Wang, Y., Wang, W., Shang, Q.H., Cao, C.Q., Erwin, D.H., 2000. Pattern of marine mass extinction near the Permian-Triassic boundary in South China. *Science* 289, 432–436.
- Jin, Y.G., Shen, S.Z., Henderson, C.M., Wang, X.D., Wang, W., Wang, Y., Cao, C.Q., Shang, Q.H., 2006a. The Global Stratotype Section and Point (GSSP) for the

- boundary between the Capitanian and Wuchiapingian stage (Permian). Episodes 29, 253–262.
- Jin, Y.G., Wang, Y., Henderson, C.M., Wardlaw, B.R., Shen, S.Z., Cao, C.Q., 2006b. The Global Boundary Stratotype Section and Point (GSSP) for the base of Changhsingian Stage (Upper Permian). Episodes 29, 175–182.
- Joachimski, M., Lai, X.L., Shen, S.Z., Jiang, H.S., Luo, G.M., Chen, B., Chen, J., Sun, Y.D., 2012. Climate warming in the latest Permian and the Permian–Triassic mass extinction. Geology 40, 195–198.
- Joachimski, M., Alekseev, A., Grigoryan, A., Gatovsky, Y.A., 2020. Siberian Trap volcanism, global warming and the Permian–Triassic mass extinction: New insights from Armenian Permian–Triassic sections. Geol. Soc. Am. Bull. 132, 427–443.
- Jost, A.B., Mundil, R., He, B., Brown, S.T., Altiner, D., Sun, Y.D., DePaolo, D.J., Payne, J.L., 2014. Constraining the cause of the end-Guadalupian extinction with coupled records of carbon and calcium isotopes. Earth Planet. Sci. Lett. 396, 201–212.
- Kershaw, S., Crasquin, S., Li, Y., Collin, P.Y., Forel, M.B., Mu, X.N., Baud, A., Wang, Y., Xie, S., Maurer, F., Guo, L., 2012. Microbialites and global environmental change across the Permian–Triassic boundary: a synthesis. Geobiology 10, 25–47.
- Korn, D., Ghaderi, A., Leda, L., Schobben, M., Ashouri, A.R., 2016. The ammonoids from the Late Permian Paratirolites Limestone of Julfa (East Azerbaijan, Iran). J. Syst. Palaeontol. 14, 841–890.
- Korn, D., Leda, L., Heuer, F., Salimi, H.M., Farshid, E., Akbari, A., Schobben, M., Ghaderi, A., Struck, U., Gliwa, J., Ware, D., Hairapetian, V., 2021a. Baghuk Mountain (Central Iran): high-resolution stratigraphy of a continuous Central Tethyan Permian–Triassic boundary section. Fossil Rec. 24, 171–192.
- Korn, D., Hairapetian, V., Ghaderi, A., Leda, L., Schobben, M., Akbari, A., 2021b. The Changhsingian (Late Permian) ammonoids from Baghuk Mountain (Central Iran). Eur. J. Taxon. 776, 1–106.
- Korte, C., Kozur, H.W., 2010. Carbon-isotope stratigraphy across the Permian–Triassic boundary: a review. J. Asian Earth Sci. 39, 215–235.
- Korte, C., Ullmann, C.V., 2018. Permian strontium isotope stratigraphy. In: Lucas, S.G., Shen, S.Z. (Eds.), The Permian Timescale. Geol. Soc. Lond. Spec. Publ. 450, 105–118.
- Korte, C., Kozur, H.W., Bruckschen, P., Veizer, J., 2003. Strontium isotope evolution of Late Permian and Triassic seawater. Geochim. Cosmochim. Acta 67, 47–62.
- Korte, C., Kozur, H.W., Joachimski, M.M., Strauss, H., Veizer, J., Schwark, L., 2004. Carbon, sulfur, oxygen and strontium isotope records, organic geochemistry and biostratigraphy across the Permian/Triassic boundary in Abadeh, Iran. Int. J. Earth Sci. 93, 565–581.
- Kozur, H.W., 1975. Beitrag zur conodontenfauna des Perm. Geol. Palaontol. Mitteilungen Innsbruck 5, 1–44.
- Kozur, H.W., 2004. Pelagic uppermost Permian and the Permian–Triassic boundary conodonts of Iran. Part I: taxonomy. Hallesches Jahrbuch Geowiss B 18, 39–68.
- Kozur, H.W., 2005. Pelagic uppermost Permian and the Permian–Triassic boundary conodonts of Iran. Part II: investigated sections and evaluation of the conodont faunas. Hallesches Jahrbuch Geowiss B 19, 49–86.
- Kozur, H.W., 2007. Biostratigraphy and event stratigraphy in Iran around the Permian–Triassic Boundary (PTB): implications for the causes of the PTB biotic crisis. Global Planet. Change 55, 155–176.
- Leda, L., Korn, D., Ghaderi, A., Hairapetian, V., Struck, U., Reimold, W.U., 2014. Lithostratigraphy and carbonate microfacies across the Permian–Triassic boundary near Julfa (NW Iran) and in the Baghuk Mountains (Central Iran). Facies 60, 295–325.
- Leonova, T.B., 2018. Permian ammonoid biostratigraphy. In: Lucas, S.G., Shen, S.Z. (Eds.), The Permian Timescale. Geol. Soc. Lond. Spec. Publ. 450, 185–203.
- Leven, E.Y., 1975. Stage table of Tethyan Permian deposits. Bull. Moscow Soc. Natural. 1, 15–21 (in Russian).
- Liu, X.C., Wang, W., Shen, S.Z., Gorgij, M.N., Ye, F.C., Zhang, Y.C., Furuyama, S., Kano, A., Chen, X.Z., 2013. Late Guadalupian to Lopingian (Permian) carbon and strontium isotopic chemostratigraphy in the Abadeh section, Central Iran. Gondw. Res. 24, 222–232.
- McArthur, J.M., Howarth, R.J., Shields, G.A., 2012. Strontium isotope stratigraphy. In: Gradstein, F.M., Ogg, J.G., Schmitz, M.D., Ogg, G.M. (Eds.), The Geological time scale 2012. Elsevier, Amsterdam, pp. 127–144.
- Mei, S.L., Wardlaw, B.R., 1996. On the Permian “liangshanensis-bitteri” Zone and the related problems. In: Wang, H.Z., Wang, X.L. (Eds.), Centennial Memorial Volume of Professor Sun Yunzhu: Stratigraphy and Palaeontology. China University of Geosciences Press, Wuhan, pp. 130–140.
- Mei, S.L., Jin, Y.G., Wardlaw, B.R., 1994a. Succession of Wuchiapingian conodonts from northeastern Sichuan and its worldwide correlation. Acta Micropalaontol. Sin. 11, 121–139.
- Mei, S.L., Jin, Y.G., Wardlaw, B.R., 1994b. Zonation of conodonts from the Maokouan–Wuchiapingian boundary strata, South China. Palaeoworld 4, 225–233.
- Mei, S.L., Jin, Y.G., Wardlaw, B.R., 1998. Conodont succession of the Guadalupian–Lopingian boundary strata in Laibin of Guangxi, China and West Texas, USA. Palaeoworld 9, 53–76.
- Mei, S.L., Henderson, C.M., Cao, C.Q., 2004. Conodont sample-population approach to defining the base of the Changhsingian Stage, Lopingian Series, Upper Permian. The palynology and micropalaeontology of boundaries. Geol. Soc. Lond. Spec. Publ. 230, 105–121.
- Nakamura, K., Golshani, F., 1981. Notes on the Permian Brachiopod Genus *Cryptospirifer*. Hokkaido University, Faculty of Science (Geology & Mineralogy), Journal (Sapporo), 4(20), pp. 67–77.
- Partoazar, H., 2002. Permian–Triassic boundary conodonts from Jolfa–Abadeh Belt along Northwest and Central Iran. Permophiles 41, 34–40.
- Payne, J.L., Turchyn, A.V., Paytan, A., DePaolo, D.J., Lehrmann, D.J., Yu, M., Wei, J.Y., 2010. Calcium isotope constraints on the end-Permian mass extinction. Proc. Natl. Acad. Sci. 107, 8543–8548.
- Rampino, M.R., Shen, S.Z., 2021. The end-Guadalupian (259.8 Ma) biodiversity crisis: the sixth major mass extinction? Hist. Biol. 33, 716–722.
- Richoz, S., Krystyn, L., Baud, A., Brandner, R., Horacek, M., Mohtat-Aghai, P., 2010. Permian–Triassic boundary interval in the Middle East (Iran and N. Oman): progressive environmental change from detailed carbonate carbon isotope marine curve and sedimentary evolution. J. Asian Earth Sci. 39, 236–253.
- Rostovtsev, K.O., Azaryan, N.R., 1973. The Permian Triassic boundary in Transcaucasia. In: LoGan, A., Hnis, L.V. (Eds.), The Permian and Triassic Systems and Their Mutual. Canadian Society of Petroleum Geologists Memoir, 2, pp. 89–99.
- Scoates, C.R., 2014. Atlas of Permian–Triassic Paleogeographic Maps, Maps 49–52, Volumes 4 of the PALEOMAP Atlasfor ArcGIS (Late Paleozoic). Mollweide Projection, PALEOMAP Project, Evanston, IL.
- Sengör, A.M.C., 1979. Mid-Mesozoic closure of Permo-Triassic Tethys and its implications. Nature 279, 590–593.
- Shahinfar, S., Yousefi Yeganeh, B., Arefifard, S., Vachard, D., Payne, J.L., 2020. Refined foraminiferal biostratigraphy of upper Wordian, Capitanian, and Wuchiapingian strata in Hambast Valley, Abadeh region (Iran), and paleobiogeographic implications. Geol. J. 55, 6255–6279.
- Shen, S.Z., Mei, S.L., 2010. Lopingian (Late Permian) high-resolution conodont biostratigraphy in Iran with comparison to South China zonation. Geol. J. 45, 135–161.
- Shen, S.Z., Shi, G.R., 2009. Latest Guadalupian brachiopods from the Guadalupian–Lopingian boundary GSSP section at Penglaitan in Laibin, Guangxi, South China and implications for the timing of the pre-Lopingian crisis. Palaeoworld 18, 152–161.
- Shen, S.Z., Gorgij, M.N., Wang, W., Zhang, Y.C., Khamar, H.R., Tanatabaei, S.H., 2009. Report of field trip of the Permian stratigraphy in Central and Eastern Iran. Permophiles 53, 2–5.
- Shen, S.Z., Henderson, C.M., Bowring, S.A., Cao, C.Q., Wang, Y., Wang, W., Zhang, H., Zhang, Y.C., Mu, L., 2010. High-resolution Lopingian (Late Permian) timescale of South China. Geol. J. 45, 122–134.
- Shen, S.Z., Crowley, J.L., Wang, Y., Bowring, S.A., Erwin, D.H., Sadler, P.M., Cao, C.Q., Rothman, D.H., Henderson, C.M., Ramezani, J., Zhang, H., Shen, Y., Wang, X.D., Wang, W., Mu, L., Li, W.Z., Tang, Y.G., Liu, X.L., Liu, L.J., Zeng, Y., Jiang, Y.F., Jin, Y.G., 2011. Calibrating the end-Permian mass extinction. Science 334, 1367–1372.
- Shen, S.Z., Cao, C.Q., Zhang, H., Bowring, S.A., Henderson, C.M., Payne, J.L., Davydov, V.I., Chen, B., Yuan, D.X., Zhang, Y.X., Wang, W., Zheng, Q.F., 2013. High-resolution  $\delta^{13}\text{C}_{\text{carb}}$  chemostratigraphy from latest Guadalupian through earliest Triassic in South China and Iran. Earth Planet. Sci. Lett. 375, 156–165.
- Shen, S.Z., Ramezani, J., Chen, J., Cao, C.Q., Erwin, D.H., Zhang, H., Xiang, L., Schoepfer, S.D., Henderson, C.M., Zheng, Q.F., Bowring, S.A., Wang, Y., Li, X.H., Wang, X.D., Yuan, D.X., Zhang, Y.C., Mu, L., Wang, J., Wu, Y.S., 2019a. A sudden end-Permian mass extinction in South China. Geol. Soc. Am. Bull. 131, 205–223.
- Shen, S.Z., Zhang, H., Zhang, Y.C., Yuan, D.X., Chen, B., He, W.H., Mu, L., Lin, W., Wang, W.Q., Chen, J., Wu, Q., Cao, C.Q., Wang, Y., Wang, X.D., 2019b. Permian integrative stratigraphy and timescale of China. Sci. China Earth Sci. 62, 154–188.
- Shen, S.Z., Yuan, D.X., Henderson, C.M., Wu, Q., Zhang, Y.C., Zhang, H., Mu, L., Ramezani, J., Wang, X.D., Lambert, L.L., Erwin, D.H., Hearst, J.M., Xiang, L., Chen, B., Fan, J.X., Wang, Y., Wang, W.Q., Qi, Y.P., Chen, J., Qie, W.K., Wang, T.T., 2020. Progress, problems and prospects: an overview of the Guadalupian Series of South China and North America. Earth Sci. Rev. 211, 103412.
- Shen, S.Z., Yuan, D.X., Zhang, Y.C., Henderson, C.M., Zheng, Q.F., Zhang, H., Zhang, M., Dai, Y., Xu, H.P., Wang, W.Q., Li, Q., Wang, Y., Wang, X.D., Mu, L., Ramezani, J., Erwin, D.H., Angiolini, L., Zhang, F.P., Hou, Z.S., Chen, J., Zhang, X.Y., Zhang, S.H., Wu, Q., Pan, Y.X., Stephenson, M., Mei, S.L., 2024. Redefinition of the Global Stratotype Section and Point (GSSP) and new Standard Auxiliary Boundary Stratotype (SABS) for the base of Wuchiapingian Stage (Lopingian Series, Permian) in South China. Episodes 47, 147–177.
- Shi, Y.K., Yang, X.N., 2005. A statistical test on diversity changes of Early and Middle Permian fusulinacean fauna in South China. Sci. China. Ser. D Earth Sci. 48, 978–984.
- Song, H.J., Wignall, P.B., Tong, J.N., Yin, H.F., 2013. Two pulses of extinction during the Permian–Triassic crisis. Nat. Geosci. 6, 52–56.
- Song, H.Y., Algeo, T.J., Song, H.J., Tong, J.N., Wignall, P.B., Bond, D.P.G., Zheng, W., Chen, X., Romaniello, S.J., Wei, H., Anbar, A.D., 2023. Global oceanic anoxia linked with the Capitanian (Middle Permian) marine mass extinction. Earth Planet. Sci. Lett. 610, 118128.
- Stanley, S.M., 2016. Estimates of the magnitudes of major marine mass extinctions in earth history. Proc. Natl. Acad. Sci. 113, E6325–E6334.
- Stanley, S.M., Yang, X.N., 1994. A double mass extinction at the end of the Paleozoic Era. Science 266, 1340–1344.
- Stepanov, D.L., 1973. The Permian System in the USSR. Permian Triassic Systems and Their Mutual Boundary Memoir, 2, pp. 120–136.
- Sun, Y.D., Farnsworth, A., Joachimski, M.M., Wignall, P.B., Krystyn, L., Bond, D.P., Ravidà, D.C.G., Valdes, P.J., 2024. Mega El Niño instigated the end-Permian mass extinction. Science 385, 1189–1195.
- Sweet, W.C., Mei, S.L., 1999. The Permian Lopingian and basal Triassic sequence in Northwest Iran. Permophiles 33, 14–18.
- Taraz, H., 1969. Permo-Triassic section in Central Iran. AAPG Bulletin 53, 688–693.
- Taraz, H., 1971. Uppermost Permian and Permo-Triassic transition beds in Central Iran. AAPG Bull. 55, 1280–1294.
- Taraz, H., 1974. Geology of the Surmag-Deh Bid Area, Abadeh region, Central Iran. Geological Survey of Iran, Report, 37, p. 148.
- Teichert, C., Kummel, B., Sweet, W., 1973. Permian-Triassic strata, Kuh-E-Ali Bashi, northwestern Iran. Bull. Museum Comp. Zool. 145, 359–472.

- Ueno, K., Tsutsumi, S., 2009. Lopingian (Late Permian) foraminiferal faunal succession of a Paleo-Tethyan mid-oceanic carbonate buildup: Shifodong Formation in the Changning-Menglian Belt, West Yunnan, Southwest China. *Island Arc* 18, 69–93.
- Ueno, K., Miyahigashi, A., Charoentirat, T., 2010. The Lopingian (Late Permian) of mid-oceanic carbonates in the Eastern Palaeotethys: stratigraphical outline and foraminiferal faunal succession. *Geol. J.* 45, 285–307.
- Viaretti, M., Crippa, G., Posenato, R., Shen, S.Z., Angiolini, L., 2021. Lopingian brachiopods from the Abadeh section (Central Iran) and their biostratigraphic implications. *Boll. Soc. Paleontol. Ital.* 60, 213–254.
- Viaretti, M., Crippa, G., Brombin, V., Porta, G.D., Griesshaber, E., Jurikova, H., Posenato, R., Bottini, C., Angiolini, L., 2025. Duration and intensity of the Late Permian (early Wuchiapingian) cool climate episode: Sclerochemical evidence from brachiopod assemblages in Iran. *Palaeogeogr. Palaeoclimatol. Palaeoecol.* 659, 112654.
- Wang, C.Y., Wang, Z.H., 1981. Permian conodont biostratigraphy of China. In: Teichert, C., Liu, L., Chen, P.J. (Eds.), *Paleontology in China*, 1979. *Geol. Soc. Am. Spec. Pap.* 187, 227–236.
- Wang, Y., Sadler, P.M., Shen, S.Z., Erwin, D.H., Zhang, Y.C., Wang, X.D., Wang, W., Crowley, J.L., Henderson, C.M., 2014. Quantifying the process and abruptness of the end-Permian mass extinction. *Paleobiology* 40, 113–129.
- Wang, W.Q., Garbelli, C., Zheng, Q.F., Chen, J., Liu, X.C., Wang, W., Shen, S.Z., 2018. Permian  $^{87}\text{Sr}/^{86}\text{Sr}$  chemostratigraphy from carbonate sequences in South China. *Palaeogeogr. Palaeoclimatol. Palaeoecol.* 500, 84–94.
- Wignall, P.B., Sun, Y.D., Bond, D.P., Izon, G., Newton, R.J., Védrine, S., Widdowson, M., Ali, J.R., Lai, X.L., Jiang, H.S., 2009. Volcanism, mass extinction, and carbon isotope fluctuations in the Middle Permian of China. *Science* 324, 1179–1182.
- Yazdi, M., Shirani, M., 2002. First research on marine and nonmarine sedimentary sequences and micropaleontologic significance across Permian/Triassic boundary in Iran (Isfahan and Abadeh). *J. China Univ. Geosci.* 13, 172–176.
- Yin, H.F., Yang, F.Q., Zhang, K.X., Yang, W.P., 1986. A proposal to the biostratigraphic criterion of Permian/Triassic boundary. *Mem. Soc. Geol. Ital.* 34, 329–344.
- Yin, H.F., Zhang, K.X., Tong, J.N., Yang, Z.Y., Wu, S.B., 2001. The Global Stratotype Section and Point (GSSP) of the Permian-Triassic boundary. *Episodes* 24, 102–114.
- Yuan, D.X., Shen, S.Z., Henderson, C.M., Chen, J., Zhang, H., Feng, H.Z., 2014. Revised conodont-based integrated high-resolution timescale for the Changhsingian Stage and end-Permian extinction interval at the Meishan sections, South China. *Lithos* 204, 220–245.
- Yuan, D.X., Chen, J., Zhang, Y.C., Zheng, Q.F., Shen, S.Z., 2015. Changhsingian conodont succession and the end-Permian mass extinction event at the Daijiagou section in Chongqing, Southwest China. *J. Asian Earth Sci.* 105, 234–251.
- Yuan, D.X., Shen, S.Z., Henderson, C.M., 2017. Revised Wuchiapingian conodont taxonomy and succession of South China. *J. Paleo.* 91, 1199–1219.
- Yuan, D.X., Shen, S.Z., Henderson, C.M., Chen, J., Zhang, H., Zheng, Q.F., Wu, H.C., 2019. Integrative timescale for the Lopingian (Late Permian): a review and update from Shansi, South China. *Earth Sci. Rev.* 188, 190–209.
- Zakharov, Y.D., Abnabi, N.M., Yazdi, M., Ghaedi, M., 2010. New species of Dzhulfian (Late Permian) ammonoids from the Hambast Formation of Central Iran. *Paleontol. J.* 44, 614–621.
- Zhang, K.X., 1987. The Permo-Triassic conodont fauna in Changxing area, Zhejiang Province and its stratigraphic significance: *Earth Science-Journal of China University of Geosciences* 12, 193–200 (in Chinese).
- Zhang, Y.C., Wang, Y., 2018. Permian fusuline biostratigraphy. In: Lucas, S.G., Shen, S.Z. (Eds.), *the Permian Timescale*. *Geol. Soc. Lond. Spec. Publ.* 450, 253–288.
- Zhang, K.X., Lai, X.L., Tong, J.N., Jiang, H.S., 2009. Progresses on study of conodont sequence for the GSSP section at Meishan, Changxing, Zhejiang province, South China. *Acta Palaeontol. Sin.* 48, 474–486.
- Zhang, F.F., Romaniello, S.J., Algeo, T.J., Lau, K.V., Clapham, M.E., Richoz, S., Herrmann, A.D., Smith, H.B., Horacek, M., Anbar, A.D., 2018. Multiple episodes of extensive marine anoxia linked to global warming and continental weathering following the latest Permian mass extinction. *Sci. Adv.* 4, e1602921.
- Zhang, M., Qin, H.F., He, K., Hou, Y.F., Zheng, Q.F., Deng, C.L., He, Y., Shen, S.Z., Zhu, R., Pan, Y.X., 2021. Magnetostratigraphy across the end-Permian mass extinction event from the Meishan sections, southeastern China. *Geology* 49, 1289–1294.
- Zhang, M., Qin, H.F., Deng, C.L., Shen, S.Z., Pan, Y.X., 2025a. A review of magnetostratigraphy around the Permian-Triassic boundary. *Global Planet Change* (in press). <https://doi.org/10.1016/j.gloplacha.2025.105022>.
- Zhang, S.H., Zhao, Y.Y., Shi, Y.K., Fang, Q., Wang, X.D., Fan, J.X., Zhang, Y.C., Yuan, D.X., Wang, Y., Zhang, F.F., Wu, H.C., Erwin, D.H., Marshall, C.R., Shen, S.Z., 2025b. Global cooling drove diversification and warming caused extinction among Carboniferous-Permian fusuline foraminifera. *Sci. Adv.* 11, eadv2549.
- Zhao, J.K., Sheng, J.Z., Yao, Z.Q., Liang, X.L., Chen, C.Z., Rui, L., Liao, Z.T., 1981. The Changhsingian and the Permian-Triassic boundary in South China. *Bull. Nanjing Inst. Geol. Palaeontol.* 2, 1–112 (in Chinese with English abstract).
- Zheng, Q.F., Cao, C.Q., Wang, Y., Zhang, H., Ding, Y., 2016. Microbialite concretions in a dolostone crust at the Permian-Triassic boundary of the Xishan section in Jiangsu Province, South China. *Palaeoworld* 25, 188–198.